REMOVAL OF LIGAND TOXICITY BY AMINO ACIDS FOR GREEN LUMINESCENT $MAPbBr_3$: A GREEN APPROACH

A DISSERTATION

Submitted for the Partial Fulfillment of the

Requirements for the award of the degree

of

MASTER OF TECHNOLOGY

in

ADVANCED METHODS OF CHEMICAL ANALYSIS

By

AJEET KUMAR SHARMA

DEPARTMENT OF CHEMISTRY

INDIAN INSTITUTE OF TECHNOLOGY ROORKEE

ROOKEE-247667 (INDIA)

MAY, 2019

CANDIDATE'S DECLARATION

I hereby declare that work is being presented in the thesis/dissertation entitled **"REMOVAL OF LIGAND TOXICITY BY AMINO ACIDS FOR GREEN LUMINESCENT $MAPbBr_3$: A GREEN APPROACH"** in partial fulfilment of the requirements for the award of the Degree **Master of Technology** in **Advance Method of Chemical Analysis** submitted in the **Department of Chemistry** of the Indian Institute of Technology Roorkee, Roorkee. This is an authentic record of my own work carried out for a period of 1 year under the supervision of **Dr. Prasenjit kar**, Assistant Professor, Department of Chemistry, Indian Institute of Technology Roorkee. The matter presented in this report has not been submitted before in any other project/thesis for the award of any other degree elsewhere.

Place: Roorkee

AJEET KUMAR SHARMA
Enrollment No. 17549001

CERTIFICATE

This is to certify that the above statement made by the candidate is correct to the best of my knowledge and belief.

Dr. Prasenjit Kar

Assistant professor

Department of Chemistry

Indian Institute of Technology Roorkee

Roorkee, Uttarakhand, India-247667

Place:

Date:

ACKNOWLEDGEMENT

I would like to express my gratefulness to my supervisor **Dr. PrasenjitKar**, Department of Chemistry, Indian Institute of Technology Roorkee for this restorative guidance, encouragement and valuable suggestions with the inspiring ideas all through this work.

I wish to express my sincere gratitude to **Prof. K. R. Justin Thomas**, Head, Department of Chemistry, Indian Institute of Technology Roorkee, **Dr. Tapas Kumar Mandal** (Coordinator for M. Tech. Programme) for giving me excellent support and guidance.

I express my gratitude to all my teachers at the department of chemistry, I wish to thank my lab-mates **Parul Bansal, Gaurav Kumar Nim, Hari Shankar Agrawal, Sukanya Ghosh, Abha Jha** and my friends **Vishakha Goyal, Abhilasha Chauhan, Ankit Sharma, Sandeep Kumar, Roquaiya Khalique** for their constant inspiration, constructive support and cooperation during the dissertation work and helping me in all possible manners. I thank my classmates for their timely help during my project work, also my heartfelt thanks to **Mr. Madan Pal** and group of their dedication in instrumentation lab. It is my pleasure to express my thankfulness to this team for helping me in collecting all the needed information and also for the help in shaping the report through their constructive, healthy suggestions and for their caring minds.

I thank I.I.T. Roorkee for providing me all the necessary facilities and MHRD, New Delhi for financial assistance.

Last but not least I am thankful to my mother, father and siblings for their constant support throughout this journey.

AJEET KUMAR SHARMA

CONTENTS

CHAPTER 3: Results

LIST OF FIGURES

LIST OF SPECTRA

LIST OF TABLES

ABSTRACT

We have reported low toxic essential amino acids as bidentate ligand for synthesis of $MAPbBr_3$ perovskite nanocrystals with excellent optical properties. This investigation shows that mechanochemical method is preferred over conventional colloidal chemistry during synthesis. To better understand the optoelectronic property, different amino acids have been studied and compared. All morphological and optical studies are performed to characterize the synthesized perovskite nanoparticles. Later, stability studies are investigated through Thermogravimetric analysis, temperature dependent PL, time dependent XRD as well XPS studies. Interestingly, these perovskites show high luminescence upon scratching on flexible conducting plates and on plain paper surface. This investigation demonstrates the importance of generating high quality fluorescent nanoparticle for photonic applications including light emitting diodes and imaging.

CHAPTER 1

1.1 INTRODUCTION OF METAL HALIDE PEROVSKITE

A composition having a crystal structure like $CaTiO_3$ is generally known as perovskite material. When Perovskite having oxygen anion, then the general formula of Perovskite structure is ABO_3 or A_2BO_4 (layered perovskite) and in case of perovskite having halide anion, the general formula is ABX_3 (X=Cl, Br, I). In the 18th century, the first time discovered calcium titanium oxide ($CaTiO_3$) mineral by Gustav Rose in the Ural Mountains of Russia. The name "Perovskite" given on the basis of great Russian mineralogist Lev Perovski. Mixed oxide type Perovskite materials like ABO_3 and A_2BO_4, are used as catalysts for NO removal[1]. First time in 1926, Perovskite's crystal structure described by Victor Goldschmidt, when he was working on tolerance factors (**t**) [2].

$$t = \frac{r_a + r_o}{\sqrt{2}(r_b + r_o)}$$

t- Tolerance Factor, r_a-Radius of A cation, r_b-Radius of B cation, r_o-Radius of O anion,

Table 1.1.1: Perovskite type oxides and their application[3],

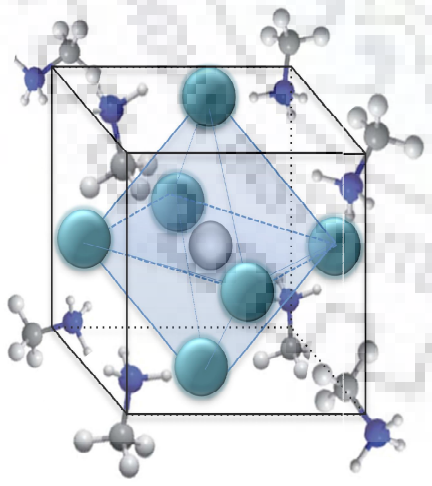

Applications	Perovskite-Type Oxides
Multilayer Capacitor	$BaTiO_3$
Piezoelectric Transducer	$Pb(Zr, Ti)O_3$
P. T. C. Thermistor	$BaTiO_3$, doped
Electrooptical Modulator	$(Pb, La)(Zr, Ti)O_3$
Switch	$LiNbO_3$
Dielectric Resonator	$BaZrO_3$
Thick Film Resistor	$BaRuO_3$
Electrostrictive Actuator	$Pb(Mg, Nb)O_3$
Superconductor	$Ba(Pb, Bi)O_3$ layered cuprates
Magnetic Bubble Memory	$GdFeO_3$
Laser host	$YAlO_3$
Ferromagnet	$(Ca, La)MnO_3$
Refractory Electrode	$LaCoO_3$
Second Harmonic Generator	$KNbO_3$

Figure 1.1.1: Perovskite structure[3],

Table 1.1.2:- Cations and Anions with their radius (nm) [4].

Cation	Radius(nm)	Cation	Radius(nm)
H^+	0.030	Zn^{2+}	0.075
Li^+	0.069	Fe^{2+}	0.078
Cu^+	0.096	V^{2+}	0.079
Na^+	0.102	Cr^{2+}	0.082
Ag^+	0.115	Mn^{2+}	0.083
K^+	0.138	Pd^{2+}	0.086
NH_4^+	0.148	Ag^{2+}	0.089
Rb^+	0.149	Sn^{2+}	0.093
Tl^+	0.150	Cd^{2+}	0.095
Cs^+	0.170	Ca^{2+}	0.100
$(CH_3)_4N^+$	0.280	Hg^{2+}	0.102
$(C_2H_5)_4N^+$	0.337	Yb^{2+}	0.105
$(C_6H_5)_4As^+$	0.428	Sr^{2+}	0.113
		Eu^{2+}	0.117
Be^{2+}	0.040	Pb^{2+}	0.118
Ni^{2+}	0.069	Sm^{2+}	0.119
Mg^{2+}	0.072	Ba^{2+}	0.136
Cu^{2+}	0.073	Ra^{2+}	0.143
Co^{2+}	0.075		

Anion	Radius(nm)	Anion	Radius(nm)
F^-	0.133	I^-	0.220
OH^-	0.133	BF_4^-	0.232
HCO_3^-	0.156	MnO_4^-	0.240
$CH_3CO_2^-$	0.162	CLO_2^-	0.240
HCO_2^-	0.169	BO_2^-	0.240
NO_3^-	0.179	ClO_4^-	0.250
IO_3^-	0.181	ReO_4^-	0.260
Cl^-	0.181	$B(C_6H_5)_4^-$	0.421
BrO_3^-	0.191		
CN^-	0.191	CO_3^{2-}	0.178
NO_2^-	0.192	S^{2-}	0.184
N_3^-	0.195	SO_3^{2-}	0.200
Br^-	0.196	SO_4^{2-}	0.230
ClO_3^-	0.200	CrO_4^{2-}	0.240
$H_2PO_4^-$	0.200	SeO_4^{2-}	0.243
OCN^-	0.203	SiF_6^{2-}	0.259
SeH^-	0.205	$PtCl_6^{2-}$	0.313
SH^-	0.207	$PdCl6^{2-}$	0.319
SCN^-	0.213	PO_4^{3-}	0.238

Organic/inorganic metal trihalide (ABX_3) perovskite has got considerable focus on the optoelectronic research community due to high photoluminescence quantum yield (PLQYs), low cost and less toxicity[5]. The use of all organic/inorganic metal trihalide perovskite NPs have demonstrated high optical absorption[6] and tunable absorption/emission wavelengths. By tuning the composition of halide ion concentration, we can enhance the development of perovskite-based NPs for applications such as solar cells[7], laser[8], light emitting diode[9] and photodetectors[10]. Organic/inorganic metal halide perovskite NPs have been synthesized by various methods generally using oleic acid, oleylamine/octylamine like mechanochemical[11], ligand-assisted reprecipitation technique[12] spin-coating[13] and inverse temperature crystallization[14]. Severely, metal halide perovskite nanoparticles (NPs) suffer from chemical and phase instabilities due to common capping ligands. Oleic acid and oleylamine forms an insulating layer by encapsulating the nanoparticles and fend their utility in optoelectronic devices. To overcome these limitations, the better option is to use bidentate ligand but the challenge still remains same i.e. ligand toxicity**.** For overcoming this toxicity, Kar *et al.* have used short bidentate ligand[15] and Bakr *et al.* have used different bidentate ligand for the synthesis of perovskite nanoparticles[16]. Generally, two individual carboxylic groups and amine-group-containing ligand are used to cap the perovskite nanoparticles. Here,

we proposed a single bidentate ligand amino acid contain both carboxylic and an amine group. Amino acid capped $CH_3NH_3PbBr_3$ nanoparticles are reported for the first-time through synthesis by mechanochemical solvent-free method. We have used different amino acids including Glycine, Alanine, Leucine, and Phenylalanine amino acids to synthesis $CH_3NH_3PbBr_3$ nanoparticles.

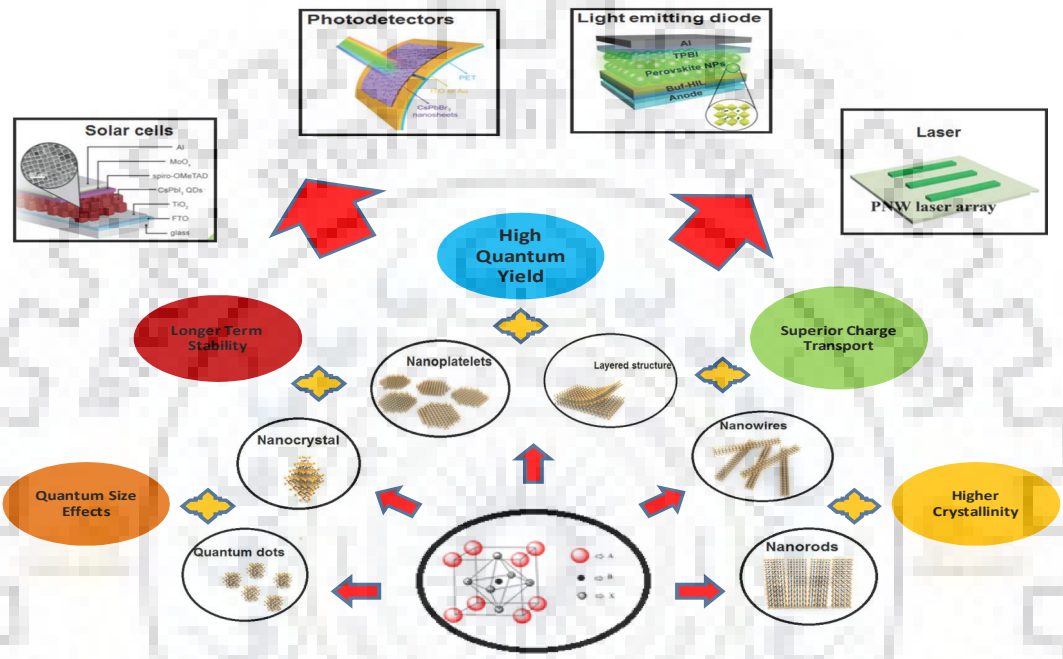

Figure 1.1.2: Different morphology of metal halide perovskite and their applications[7].

1.2 QUANTUM SIZE EFFECT IN METAL HALIDE PEROVSKITE:-

Quantum dots are tiny particles or NCs (nanocrystals) of a semiconducting material with diameters in the range of 2-10 nanometers. Quantum dots were first time discovered in 1980[17]. Quantum dots displays unique electronic properties, and these are intermediate between those of bulk semiconductors and discrete molecules. That is partly the result of the unusually high surface-to-volume ratios for these particles[18]. The most apparent result of these perovskite nanoparticles is fluorescence. Quantum dots being nicknamed as 'artificial atoms'. Generally, It is found that the size of the crystal decreases, the difference in energy between the highest valence band (VB) and the lowest conduction band (CB) increases. So more energy is needed to excite the dot, and more energy is released when the crystal returns to its ground state, resulting in a color shift from red to blue in the emitted light. As a result of

this phenomenon, quantum dots can emit any color of light from the same material simply by changing the dot size.

Jasmina A. Sichert *et al.* explained the quantum size effect in Organometal Halide Perovskite nanoplatelets. In this article, we can monitor the thickness of organometal halide perovskite platelets by controlling the ratio of organic ligands used in the synthesis. It was found that as the fraction of the large organic cation like OA (octyl ammonium) increased, the thickness of the perovskite nanoplatelets decreases to single octahedral (Oh). Quantum confinement in semiconductor nanostructures is generally determined by effective mass approximation which is based on two factors, the size of nanostructure (d) and exciton Bohr radius (a_B). If $d >> a_B$, an excited electron and hole pair binds together forming an exciton. And, if $a_B >> d$, this is the indication of strong confinement regime and electron-hole need to be viewed as separate particles[19]. In peculiar, the optical properties of metal halide perovskite (ABX_3, A=Organic or Inorganic cation, X=Cl, Br, I) can be widely framed up once its bulk structure has been reduced to low dimensional Structure such as 0D, 1D, 2D.

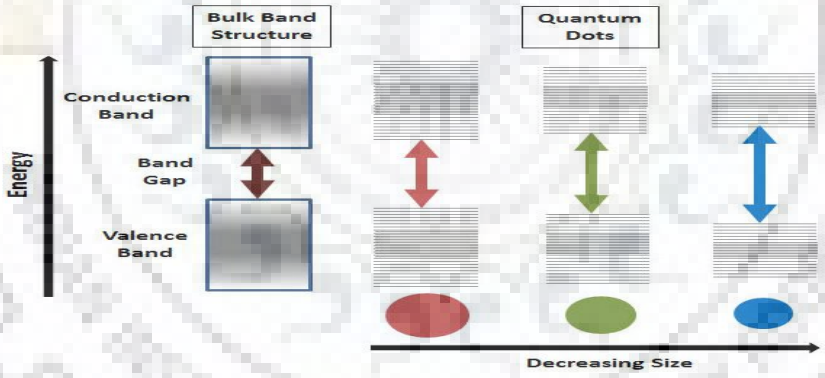

Figure 1.2.1: Quantum size effect[19].

1.3 COMMON SYNTHESIS METHODS OF PEROVSKITE QDs:-

Perovskite QDs generally synthesized by three common synthesis methods, (1) Ligand assisted reprecipitation method, (2) Hot Injection method and (3) Mechanochemical synthesis. These methods are widely used for the preparation of perovskite with different morphology. Out of these, mechanochemical synthesis is one with solvent-free synthesis.

1.3.1 LIGAND ASSISTED REPRECIPITATION METHOD (LARP):-

Yuping Dong *et al.*[20] synthesized $CH_3NH_3PbX_3$ (X=Cl, Br, I) QDs by ligand assisted reprecipitation method (LARP). In this method CH_3NH_3X, PbX_2, and long chain ligands (Oleic acid and Octylamine) are dissolved in a good solvent like N-dimethylformamide (DMF) to make a precursor solution. DMF is a good solvent because it dissolves inorganic salts and small molecules. This precursor solution dissolves in poor or bad solvent (Toluene, Hexane, etc.) with continuous stirring. In this synthesis, oleic acid and octylamine used as long chain ligands. Basically, octylamine controls the kinetics of crystallization (due to which fast crystallization and aggregation do not take place result in small particles) and oleic acid controls the colloidal stability. They found emission peaks from 407 nm to 734 nm by tuning the halide composition. This organic lead halide ($CH_3NH_3PbX_3$) perovskite QDs used in Display technology.

1.3.2 HOT INJECTION METHOD:-

Maksym V. Kovalenko *et al.*[21] synthesized $CsPbX_3$ (X=Cl, Br, I) nanocrystals by hot injection method. In this method, prepare a Cs-Oleate precursor solution by Cs_2CO_3 and Oleic acid reaction in octadecene for 1 h at 120 °C under nitrogen atmosphere. In another flask, PbX_2 dried under vacuum for 1h at 120 °C, add oleic acid and oleylamine under nitrogen atmosphere at 120 °C for 1h. When the sublimation process of PbX_2 is completed, add quickly Cs-Oleate and further heat it for 5 min at 150 °C, resulting in formation of nanocrystals. PL emission peaks showed at 410-530 nm corresponds to blue-green emission peaks by mixing of $PbCl_2$ and $PbBr_2$. Inorganic lead halide ($CsPbX_3$) perovskite showed 50-90% PLQYs. $CsPbX_3$ perovskite synthesized by this method, covering up to 140% of the color gamut of NTSC (National Television System Committee) color standard.

1.3.3 MECHANOCHEMICAL SYNTHESIS METHOD:-

Sameer Sapra *et al.*[22] synthesized organic-inorganic lead bromide perovskite bulk and nanoparticles at room temperature by mechanochemical synthesis method. This synthesis method is also known as a solvent-free method. In this method simply grind the precursors including $PbBr_2$, MABr/ FABr/ Cs along with appropriate capping ligands like oleic acid and oleylamine to synthesis $MAPbBr_3$ or $FAPbBr_3$ or $CsPbBr_3$ perovskite nanoparticles. These

are characterized by powder XRD and TEM analysis. It was also investigated that thermal stability order of these nanoparticles is $CsPbBr_3$>$MAPbBr_3$>$FAPbBr_3$.

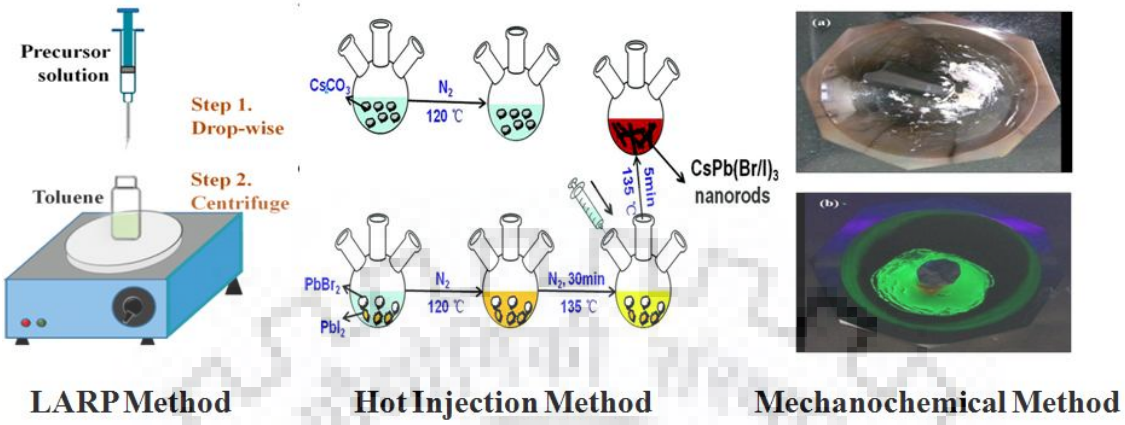

Figure 1.3.1: Common Synthesis methods of metal halide perovskite[20].

1.4. ROLE OF SOLVENT IN METAL HALIDE PEROVSKITE:-

Solvent plays a crucial role in the formation of high-quality solution processed perovskite films. Solvents are not only dissolving the solute but also participate in the crystallization of perovskite, controlling morphology, widening process window and controlling the nuclei/growth.

In one step method, lead halide (PbX_2, X=Cl, Br, I) and AX (A=Methylammonium, Formamidinium) is dissolved into a polar aprotic solvent like DMF, DMSO, GBL or NMP to form a precursor solution. This precursor solution is then coated onto a substrate and by removing the residual solvent, perovskite film is formed. In this method solvent is controlling the morphology, As the volume of DMF solvent increases from 20 to 100 µL, morphology changes from nanoparticles to nanowires[23]. In the two-step method, perovskite film is formed in a two-step. In this method first PbI_2 dissolves in DMF to form a solution and form PbI_2 films. Then these PbI_2 films react with MAI to form $MAPbI_3$ perovskite films. In two-step method, solvent fuction is controlling the Nuclei/growth of metal halide perovskite[24].

1.5 ROLE OF LIGANDS IN METAL HALIDE PEROVSKITE:-

Christoph J. Brabec *et al.*[25] synthesized $CH_3NH_3PbX_3$ (X=Br, I) perovskite nanoplatelets. The thickness of these platelets in between 1-8 unit cell monolayers, that depend on the ratio of common capping ligands oleic acid and oleylamine. When oleic acid (OA) and oleylamine (OAm) ratio was 200µL/16 µL, they found 89% PLQY, 2.6±0.2 thickness of platelets and 2.36 eV band gap. When OA/OAm ratio was 200µL/21 µL, then 50% PLQY, 2±0.1 thickness of platelets and 2.59 eV band gap. When OA/OAm ratio was 200µL/30 µL, then 32% PLQY, 1.6±0.1 thickness of platelets and 2.74 eV band gap. **Zhengtao Deng** *et al.*[26] synthesized $CsPbX_3$ (X=Cl, Br, I) by ligand-mediated reprecipitation strategy at ordinary temperature. When they used hexanoic acid - octylamine, oleic acid - dodecylamine, acetate acid - dodecylamine and oleic acid - octylamine, these formed quantum dots, nanocubes, nanorods and nanoplatelets morphology, respectively. **Osman M. Bakr** *et al.*[27] used 2,2'-iminodibenzoic acid (IDA) as a bidentate ligand to passivate $CsPbI_3$ perovskite nanocrystals because common capping ligand (Oleic acid and Oleylamine) formed an insulating layer. **Jin Z. Zhang** *et al.*[28] synthesized $CH_3NH_3PbBr_3$ perovskite NCs using straight chain ligands (octylamine, octyl ammonium bromide) and branched capping ligands (3-aminopropyl triethoxysilane, polyhedral oligomeric silsesquioxane). As the branching increases steric hindrance increases due to which they protect PNCs from dissolution by DMF. **Nan Ma** *et al.*[29] synthesized $CsPbBr_3$ nanoplatelets using oleic acid, oleylamine and different concentrations of tryptophan (amino acid). They found that as the concentration of tryptophan increases, the formation of nanoplatelets increases.

1.6 LOW DIMENSIONAL METAL HALIDE PEROVSKITE:-

Due to the solar cell, LED, photodetector, waveguide and nanolaser applications of low dimensional perovskite. They attracted considerable attention of research community. So the research community focusing on a new shape, size and thickness controlled synthesis methods. Quantum dots (QDs), Nanoparticles (NPs), Nanowires (NWs), Nanorods, Nanoplates, Nanosheets are various morphologies of low dimensional perovskite.

1.6.1 0DPs: QUANTUM DOTS (QDs)

Quantum dots (QDs) are tiny spherical particles, size lies in between 1-10 nm range. Two methods, Hot injection and Ligand assisted re-precipitation method are most commonly used

for the synthesis of 0D perovskite-like quantum dots (QDs). Size-controlled optical properties of quantum dots (QDs) are wacky features. **H. Huang** *et al.*[30] synthesized $CH_3NH_3PbBr_3$ QDs at different precipitation temperature and also studied the temperature dependent PL, UV and average decay lifetimes study of $CH_3NH_3PbBr_3$ QDs. They found that Optical absorption and emission spectra were red shifted as temperature increases. Quantum yields (QYs) increase as temperature increase and average decay lifetimes (τ_{avg}) of $CH_3NH_3PbBr_3$ QDs decrease as temperature increases.

1.6.2 1DPs: NANOWIRES, NANORODS

One dimensional morphology (Nanowires, Nanorods) is used in optoelectronic devices (LEDs, Solar cell). **Yang** *et al.*[31] introduced room temperature growth of nanorod arrays and low temperature anion exchange technique. In room temperature growth technique, they successfully growed nanorods of $CH_3NH_3PbBr_3$. In low temperature anion exchange technique, $CH_3NH_3PbBr_3$ nanorod arrays were converted into $CH_3NH_3PbI_3$ nanorod arrays. **Nam Gyu Park** *et al.*[32] synthesized $CH_3NH_3PbI_3$ nanowire using an aprotic solvent in the two-step spin coating method. They have explained the effect of aprotic DMF in isopropanol MAI solution. As the volume of DMF increases in MAI isopropanol solution, the first fused nanoparticles are formed then nanowires thickness increases. They found that nanowires density increase on increasing the concentration of MAI by keeping the volume constant of DMF. They also explain the effect of aprotic solvent like DMF, GBL, DMSO. When they used DMF, well define nanowire formed and on using GBL or DMSO, well define nanowire were not form.

1.6.3 2DPs: NANOPLATELETS, NANOSHEETS

Two dimensional perovskite are ionic materials and fabricated by solution phase synthesis as well as the vapor phase deposition technique. **Alivisatos, A. P.** *et al.*[33] synthesize $CsPbX_3$ nanoplatelets with the 84% PLQYs. They have observed temperature play a crucial role in the shape and thickness of nanoplatelets. **Qiaoliang Bao** *et al.*[34] synthesize organic-inorganic two-dimensional hybrid perovskites ($CH_3NH_3PbI_3$) using the combined solution process and vapor phase conversion method.

1.7 DEGRADATION MECHANISM OF METAL HALIDE PEROVSKITES

Yongli Gao and co-workers[35] reported a degradation process of $MAPbBr_3$ single crystal in X-ray, H_2O, O_2 and N_2 environment in a UHV system. In X-ray exposure, the HR-XPS technique was used. This HR-XPS technique identifies metallic Pb. In O_2 and N_2 exposure, N_2 generally is used as an inert gas to protect sample but N_2 and O_2 exposure on $MAPbBr_3$ from $0\text{-}10^{12}$ L acted as p-type dopants. The difference is that nitrogen was physically absorbed and slowly escaped the surface, but oxygen formed a C-O bond with carbon. In H_2O exposure, H_2O works as an n-type dopant and starts to react with the $MAPbBr_3$ surface. **N. Rajamanickam** *et al.*[36] proposed possible degradation or decomposition route of MAPbI3 in the influence of water, oxygen, and UV.

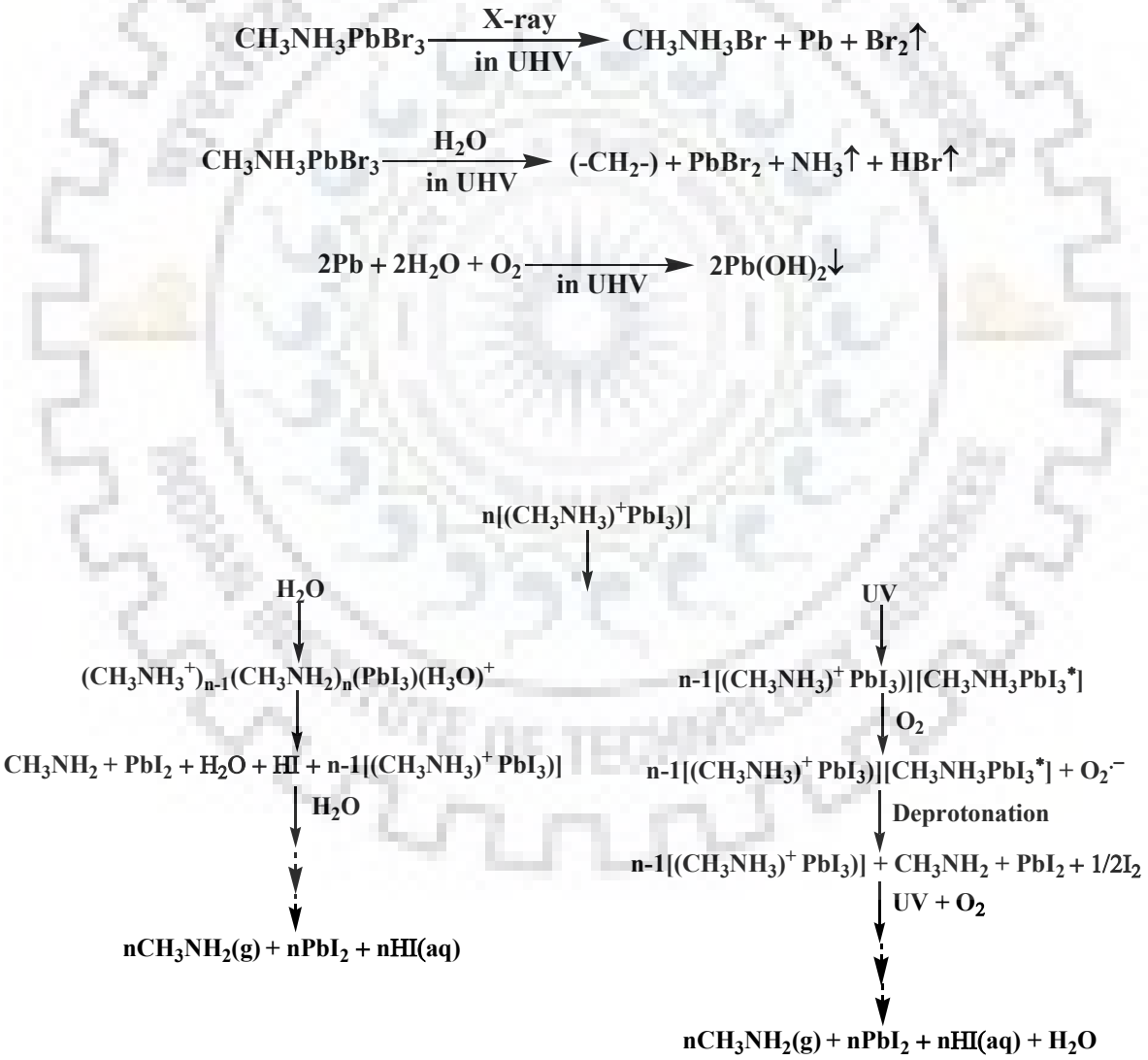

1.8 APPLICATIONS OF METAL HALIDE PEROVSKITE

In last few decades lead halide perovskite materials, $A^{I}Pb^{II}X_3$ (A = Cs , CH_3NH_3; X = Cl, Br, I) with high photoluminescence quantum yield (PLQY) have been demonstrated as an efficient applier for photovoltaic (PV) applications. This is because of its suitable band gap, high absorption coefficient, defect tolerant nature, high charge carrier mobility and long diffusion length. Due to tunable emission in the visible region and power conversion efficiency (PCE) up to 23% have made it as a potential candidate for various optoelectronic applications such as light emitting diodes (LED), lasing and non linear optics. Recently Arindam Chowdhury *et al* and their group has showed that $MAPbBr_3$ in its micro crystalline form having high fluorescence and reasonable fluorescence life time of 51 ns is applicable as a fluorescence blink. These types of materials can also be used as fluorescence ink and keypad lock. This can be said by the report of Prasenjit Kar *et al* and their group. Metal halide perovskite has established itself as a potential candidate for organic dye degradation. Furthermore, we started a proof of concept experiment by coating perovskite nanocrystals onto the paper and flexible conductive surface. After coating the substrate surface, letters 'IIT" were written by simply scratching on it as shown in Figure 1.8.1. While the application of PL paper is seldom reported, the paper coated with nanocrystals can be applied as rewritable PL paper as shown in scheme (Fig. 1.8.1).

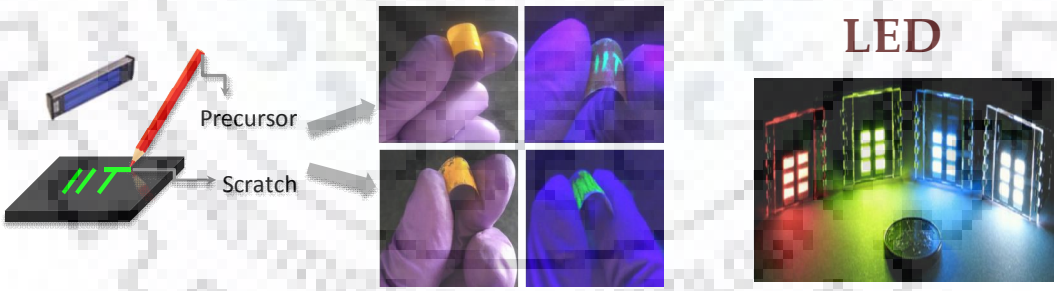

Figure 1.8.1: Schematic illustration of mechanochromic luminescent paper at day light and under UV light (top) and flexible conductive surface at day light and under UV light (bottom).

1.9 LITERATURE SURVEY

Various methods for the synthesis, fabrication, metal doping, Pb free perovskite, and degradation of Perovskite, etc have been reported in the literature. A number of reports are

available on the usage of different ligand but ligand toxicity still remains a challenge for the research community. A brief review of some more important studies have been included in this report and classified as;

Tsutomu Miyasaka *et al.*[37] have synthesized first time $CH_3NH_3PbBr_3$ and $CH_3NH_3PbI_3$ nanocrystalline particles on the TiO_2 surface with the power conversion efficiency 3.13% and 3.81% respectively. They studied incident photon to current quantum conversion efficiency (IPCE) and photocurrent-voltage (I-V) action spectrum of $CH_3NH_3PbBr_3/TiO_2$ and $CH_3NH_3PbI_3/TiO_2$. $CH_3NH_3PbBr_3/TiO_2$ and $CH_3NH_3PbI_3/TiO_2$ synthesized cell showed open circuit voltage (Voc) value, 0.96 V and 0.6 V respectively.

Sang Seok *et al.*[38] have reported the two-step deposition method for the fabrication of Perovskite solar cells (PSCs). In this method, the composition of $FAPbI_3$ is manipulated by adding a small amount of $MAPbBr_3$. The tuning in composition is performed by taking a 95/5 ratio of $PbI_2/PbBr_2$. In the first step, $PbI_2/PbBr_2$ dissolved in a mixture of DMF and DMSO onto the nanocrystalline TiO_2 surface. In the second step, FAI/MABr dissolved in isopropyl alcohol (IPA) containing 1-5 mmol of iodide ions (I^-) solution. The performance of perovskite solar cell (PSCs) depend on the addition of I_3^- ions to the dripping solution, because when 3 mmol of I_3^- used (Target layer) to show high PSCs efficiency and when 0 mmol of I_3^- used (Control layer) to show low PSCs efficiency. They studied 80 perovskite solar cells (PSCs) independently under the same experimental condition and found average perovskite cells efficiency (PCE) 21.25±1.08%.

David S. Ginger *et al.*[39] have synthesized $MAPbI_3$ using Lewis base to enhance photoluminescent (PL) lifetime (ι) and photoluminescent quantum efficiency (PLQE), because Lewis base acting as an electron donor. Some researchers group also used a Lewis base (pyridine improve PL brightness) and acid to improve solar cell efficiency by reducing defects. David S. Ginger *et al.* used a Lewis base like tri-n-octylphosphine oxide (TOPO), 1-octadecanethiol (ODT) and triphenylphosphine (PPh_3) acted as a monodentate ligand.

Yi Liu *et al.*[40] have synthesized $CsPbBr_3$ perovskite nanoparticles using CsOAc instead of Cs_2CO_3 due to solubility issues, because CsOAc is more soluble in octadecene (ODE) than Cs_2CO_3. They investigated the surface ligands effect on morphology by tuning the chain length of carboxylic acid and amine as well as temperature. At low temperature (140 °C), when chain length of amine increase with oleic acid morphology changes from

thinner nanoplatelets to thicker nanoplatelets. At high temperature (170 °C), when chain length of amine increase with oleic acid morphology changes from nanoplatelets to nanotubes. At low temperature (140 °C), when chain length of acid increases with oleylamine morphology changes from nanoplatelets to nanoplatelets. At high temperature (170 °C), when chain length of acid increases with oleylamine morphology changes from large nanocubes to small nanocubes.

Nam Gyu Park *et al.*[41] have fabricated $MAPbI_3$ by Lewis base adduct. The fabrication process carried out by taking MAI + PbI_2 and MAI + PbI_2 + DMSO in DMF solvent. They found S=O stretching frequency 1045 cm^{-1}, 1020 cm^{-1} and 1015 cm^{-1} corresponding to ligand DMSO, PbI_2.DMSO and MAI.PbI_2.DMSO adduct. When they heated MAI.PbI_2.DMSO in DMF at 65°C for 1 min due to rapid evaporation of DMF, $MAPbI_3$ film form. To overcome this rapid evaporation they used diethyl ether. They found avg power conversion efficiency (PCE) 18.3% by analyzing 41 cells.

Lioz Etgar *et al.*[42] have prepared cubic $MAPbX_3$ (X = Br, I) using MAX and PbX_2 in the DMF solution. The reaction carried out in octadecene at 80 °C taking oleic acid and different alkylammonium chain length ligands. They used octyl ammonium (C8), dodecyl ammonium (C12) and octadecylammonium (C18) as alkylammonium chain length ligands. They found PLQYs 30-80% depending on halide ion and alkylammonium chain length. They observed high PLQY in the case of bromide nanoparticles (NPs) with shorter alkylammonium chain length C8 as compare to iodide nanoparticles (NPs).

Edward H. Sargent *et al.*[43] have synthesized $CsPbX_3$ (X=Cl, Br, I) perovskite quantum dots (PQDs) by taking solely oleic acid. Some researcher showed that during purification of PQDs degradation take place due to proton transfer between oleic acid and oleylamine surface. They synthesized $CsPbX_3$ in two steps, (1) mixing of Cs-acetate, Pb-acetate, octadecene (ODE), oleic acid in flask and heat at 120 °C until CsOA (Cs-oleate), $PbOA_2$ (Pb-oleate) formed, (2) Put this flask in N_2 atmosphere, temperature cool down to 75 °C and added tetraoctylammonium halide (TOAX). Here results show the color changes from colorless to a green, indication of the formation of $CsPbBr_3$. They found, $CsPbBr_3$, $CsPb(Cl,Br)_3$ PQDs show high stability over a time however $CsPb(Br,I)_3$ PQDs unstable.

Prasenjit Kar *et al.*[44] have synthesized $CH_3NH_3PbBr_3$ NPs using succinic acid and oleylamine, one step towards short chain ligands is approached because of ravelling succinic acid in place of oleic acid. They have synthesized $CH_3NH_3PbBr_3$ NPs by the LARP method

And characterized $CH_3NH_3PbBr_3$ NPs by UV, PL, XRD, XPS, TEM, TCSPC and CIE coordinate. They studied time-dependent PL of $CH_3NH_3PbBr_3$ Perovskite solution containing 400 μL water.

Liberato Manna *et al.*[45] have proposed a change in the dimensionality of $CsPbBr_3$ by using amines. They found morphology changes from 3D to 0D by using butylamine (BuAm). This transformation changes by the deficiency of $PbBr_2$ from $CsPbBr_3$ (3D morphology). In morphology transformation, when TMEDA used rapid transformation take place whereas amino acid used slow transformation take place due to the low affinity of amino acid toward $PbBr_2$. TEM images explained the transformation of CsPbBr3 NCs (3D) orthorhombic transformed into Cs_4PbBr_6 (0D) and 0D to 3D transformation take place by annealing at 100 °C.

Maksym V. Kovalenko *et al.*[46] have used zwitterionic capping ligand for the stability of colloidal $CsPbX_3$ (X=Cl, Br, I) nanocrystals (NCs). They used zwitterionic capping ligand in place of common capping ligand oleic acid - oleylamine. They used 3-(N, N-dimethyloctadecylammonio)-propanesulfonate, N-hexadecylphosphocholine, and N, N-dimethyldodecylammoniumbutyrate as zwitterionic capping ligands. These ligands passivate the cation and anion surface. These zwitterionic ligands also enhanced thermal and environmental stability.

Joseph M. Luther *et al.*[47] have demonstrated ligand exchange chemistry on the $CsPbI_3$ quantum dots (QDs) surface. They synthesized $CsPbI_3$ quantum dots (QDs) by the hot injection method and purified by the MeOAc along with hexane. They found that the hydrolysis of an ester gives carboxylic acid and alcohol. First, anionic ligand exchange reaction occurred between oleate bounded $CsPbI_3$ QDs and protonated acetic acid yield acetate bound QDs, free oleic acid, and methanol. The second cationic ligand exchange reaction have occurred between oleylammonium bound QDs and cationic species.

Xue Bo Yin *et al.*[48] have prepared first time intrinsic and tunable emission color metal-organic frameworks (MOFs) with the help of 5-boronoisophthalic acid (5-bop). They have used Eu^{3+}, Tb^{3+}, Dy^{3+}, and Ln^{3+} to obtain color emissions by tuning the ratio of these metal ions. Out of these metal ions, Tb^{3+} and Dy^{3+} were most required for the formation of MOFs. All Ln^{3+} ions with isophthalic acid (ISP) do not form MOFs whereas the addition of boric acid in ISP promotes the formation of MOFs by improving steric hindrance and hydrogen bonding.

CHAPTER 2

2 EXPERIMENTAL SECTION

2.1 Chemicals list

2.1 Table: Chemicals with grade and suppliers,

Sr.No.	Chemicals	Supplier	Grade
1.	Acetone	Rankem	LR
2.	Chloroform	Thomas Baker	AR
3.	Methyl amine	Aldrich	AR
4.	Hydrobromic acid	SRL	LR
5.	Oleylamine	Aldrich	AR
6.	Oleic Acid	Chemlabs	AR
7.	Lead Bromide	Aldrich	AR
8.	Toulene	Thomas Baker	AR
9.	Oxalic Acid	Himedia	AR
10.	Tartaric Acid	Himedia	AR
11.	L-Glycine	Aldrich	AR
12.	L-Alanine	Himedia	AR
13.	L-Leucine	Himedia	AR
14.	L-Phenylalanine	Himedia	AR

2.2. INSTRUMENTATION DETAILS,

2.2.1 UV-Vis Absorption Spectroscopy was used to record UV-Vis absorption spectra in the range of 200-750 nm by Shimadzu UV-Vis 2450 spectrophotometer.

2.2.2 Photoluminescence (PL) spectra were recorded by Horiba Scientific Fluoromax-4C spectrophotometer.

2.2.3 Fourier-Transform Infrared Spectroscopy was used to record infra red spectrum of material using Thermo Scientific Nicolet 6700.

2.2.4 Powder XRD was recorded with Bruker D8 Advance diffractometer having target source Cu and accelerating voltage of 40kV from 10° to 60° with scanning rate of 2°/min.

2.2.5 Nuclear Magnetic Resonance Spectroscopy was used to record ^{1}H NMR in $DMSO_{d\text{-}6}$ with TMS (0 ppm) as internal standard and ^{13}C solid NMR spectra on a 400 MHz NMR Spectrometer.

2.2.6 X-Ray Photoelectron Spectroscopy (XPS) was used to determine elemental composition of the surface of compounds with a photoelectron spectrometer PHI 5000 VersaProve III.

2.2.7 Thermogravimetric Analysis (TGA) of powder sample was performed under inert nitrogen atmosphere at a heating rate of 10 °C/min.

2.2.8 Atomic Force Microscopy was used to perform surface analysis by model no. NT-MDT-INTEGRA AFM instrument in tapping mode.

2.2.9 FE-SEM Carl Zeiss Ultra Plus was used to analyze surface morphology of sample at 20kV.

2.2.10 Transmission Electron Microscopy (TEM) was used to analyze surface morphology of dilute sample placed on carbon coated copper grid by FEI TECHNAI G^2 20 S-TWIN electron microscope.

2.3 SYNTHETIC PROCEDURE,

$CH_3NH_3PbBr_3$ NPs is synthesized by the mechanochemical solvent free method using Bidentate ligand. Lead bromide (0.00367 g, 0.01 nmol), Methylamine hydrobromide (0.0011 g, 0.01 mmol) and X mmol of Glycine/Alanine/Leucine/Phenylalanine bidentate ligand in 1:1:X molar ratio were grinded with the help of mortar pestle for 9-20 mins. Green luminescent $CH_3NH_3PbBr_3$ NPs were obserbved under UV light.

2.3.1 Methylammonium Bromide (MABr) synthesis. In a 50 ml flask, 6 ml CH_3NH_2 40% in methanol, was mixed with 5 ml of ethanol. Then, at room temperature, 5 ml of the HBr was added along with stirring. Rotary evaporator is used for removing all solvents. Washing was done with ethylether. Re-crystallised product was obtained by dissolving it in ethanol and later using diethyl ether.

2.3.2 Synthesis of PNC-L

0.01 mmol of CH_3NH_3Br, 0.01 mmol of $PbBr_2$ and 0.01 mmol of Leucine were grinded in mortar pestle for 15-20 minutes. Green luminescent powder was obtained (under UV chamber).

2.3.3 Synthesis of PNC-P

0.01 mmol of CH_3NH_3Br, 0.01 mmol of $PbBr_2$ and 0.0035 mmol of Phenylalanine were grinded in mortar pestle for 12-18 minutes. Green luminescent powder was obtained (under UV chamber).

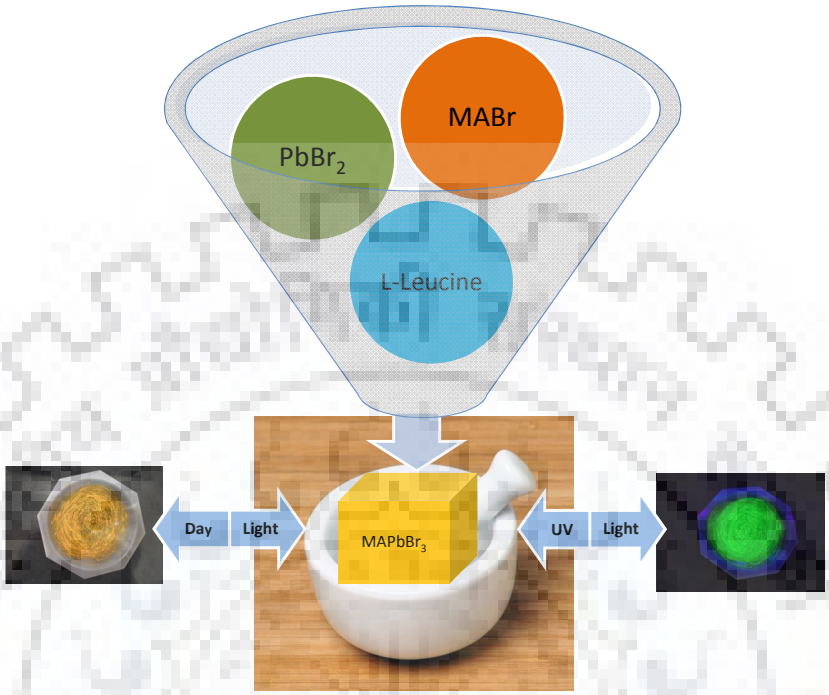

Figure 2.3.1: $CH_3NH_3PbBr_3$ PNCs synthesis scheme

Figure 2.3.2: (a) $CH_3NH_3PbBr_3$ with out Leucine, (b) $CH_3NH_3PbBr_3$ with Leucine.

CHAPTER 3

3. RESULTS AND DISCUSSIONS

We have synthesized and characterized $CH_3NH_3PbBr_3$ perovskite NPs using bidentate ligand.

3.1 Synthesis of $CH_3NH_3PbBr_3$ perovskite using dicarboxylic group containing ligand

We have synthesized $CH_3NH_3PbBr_3$ perovskite by taking oxalic acid or tartaric acid with oleylamine or octylamine. Lead bromide (0.0367 g, 0.1 nmol), Methylamine hydrobromide (0.011 g, 0.1 mmol), Oxalic acid (0.0091 g, 0.1 mmol) or Tartaric acid (0.015 g, 0.1 nmol) and Oleylamine (200 μL) or Octylamine (200 μL) were used to synthesize $CH_3NH_3PbBr_3$ perovskite by LARP and Mechanochemical method as shown below in Table 3.1.1 and Table 3.1.2.

Table 3.1.1: Synthesis of $CH_3NH_3PbBr_3$ PNCs using oxalic acid as bidentate ligand.

METHOD	PEROVSKITE	LIGANDS	RESULT
Mechanochemical	$MAPbBr_3$	Oxalic acid	No fluorescence
Mechanochemical	$MAPbBr_3$	Oxalic acid+Oleylamine	No fluorescence
Mechanochemical	$MAPbBr_3$	Oxalic acid+Octylamine	No fluorescence
LARP	$MAPbBr_3$	Oxalic acid+ Oleylamine	No fluorescence

Table 3.1.2: Synthesis of $CH_3NH_3PbBr_3$ PNCs using tartaric acid as bidentate ligand.

METHOD	PEROVSKITE	LIGANDS	RESULT
Mechanochemical	$MAPbBr_3$	Tartaric acid + Oleylamine	low fluorescence
LARP	$MAPbBr_3$	Tartaric acid + Oleylamine	No fluorescence

3.2 Synthesis of $CH_3NH_3PbBr_3$ PNCs using amino acid as bidentate ligand

We have again synthesized four different $CH_3NH_3PbBr_3$ perovskites by capping with Glycine, Alanine, Leucine and phenylalanine as bidentate ligands. By taking 1:1:1 ratio of Lead bromide (0.0036 g, 0.01 mmol), Methylamine hydrobromide (0.0011 g, 0.01 mmol) and Glycine (0.0007 g, 0.01mmol) or Alanine (0.0009 g, 0.01mmol) or Leucine (0.0013 g, 0.01

mmol) were grinded in mortar pestle by mechanochemical solvent free method for 12-15 min at room temperature. PNC-L stand for synthesis of $CH_3NH_3PbBr_3$ perovskites using Leucine. PNC-P, PNC-G and PNC-A stand for synthesis of $CH_3NH_3PbBr_3$ perovskites using Phenylalanine, Glycine and Alanine, respectively.

Phenylalanine is used as capping ligand for the synthesis of $CH_3NH_3PbBr_3$ perovskite by mechanochemical method. Lead bromide (0.0036 g, 0.01 mmol), Methylamine hydrobromide (0.0011 g, 0.01 mmol) and Phenylalanine (0.0006 g, 0.0035 mmol) were grinded in mortar pestle for 9-12 min. The green fluorescence order under UV chamber was found to be Glycine<Alanine<Leucine<Phenylalanine.

3.2 Spectral Characterization studies of $CH_3NH_3PbBr_3$ PNCs using amino acids

3.2.1 Concentration Optimization of $MAPbBr_3$ PNCs using Amino acids as Capping Ligands

Concentration of Leucine and Phenylalanine was optimized for capping of $CH_3NH_3PbBr_3$ perovskite NPs by mechanochemical method. Keeping the concentration of Lead bromide (0.0036 g, 0.01 mmol) and Methylamine hydrobromide (0.0011 g, 0.01 mmol) constant, we had varied concentration of Leucine and Phenylalanine. Concentration of leucine and phenylalanine was found as 0.01 mmol and 0.0035 mmol, which was the optimized concentration respectively shown in Figure 3.2.1.1 and 3.2.1.2.

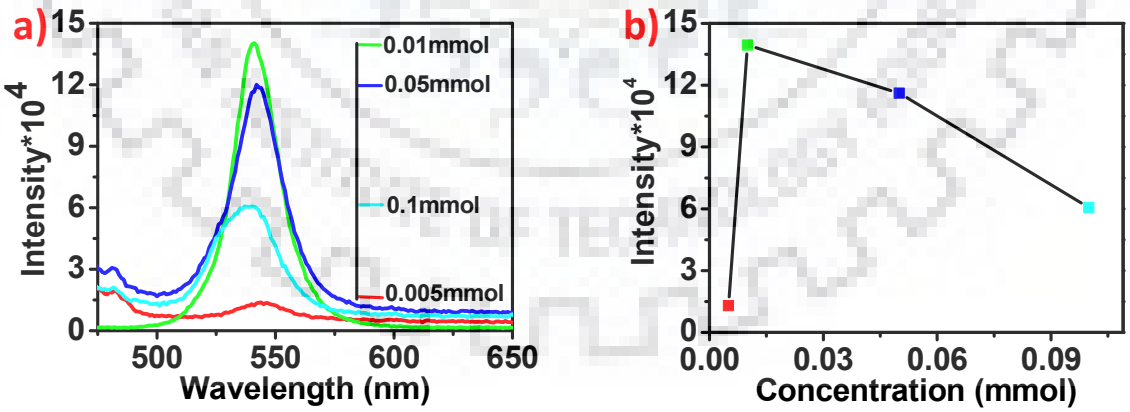

Figure 3.2.1.1: a) Photoluminescence (PL) studies of PNC-L using different concentration of Leucine ligand, b) PL intensity versus concentration (mmol) plot of PNC-L.

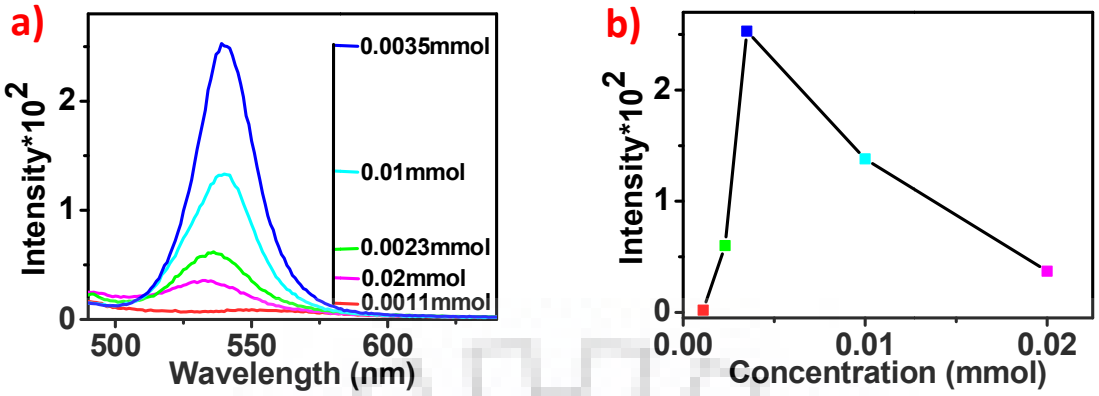

Figure 3.2.1.2: a) Photoluminescence studies of PNC-P using different concentration of Phenylalanine ligand, b) PL intensity versus concentration (mmol) plot of PNC-P.

3.2.2 Grinding Time Optimization of $MAPbBr_3$ PNCs using amino acids as Capping Ligands

Grinding time optimization studies of PNC-L and PNC-P were carried out at room temperature by photoluminescence spectroscopy. We have taken PL spectra of PNC-L and PNC-P at an interval of 3 minutes. We have also taken images of PNC-L and PNC-P at an interval of 3 minutes during grinding shown in Figure 3.2.2.1. We had found that as the grinding time increase, PL intensity increases. Grinding time was found to be optimized as 12 minutes and 9 minutes for PNC-L and PNC- P, respectively as shown in Figure 3.2.2.2.

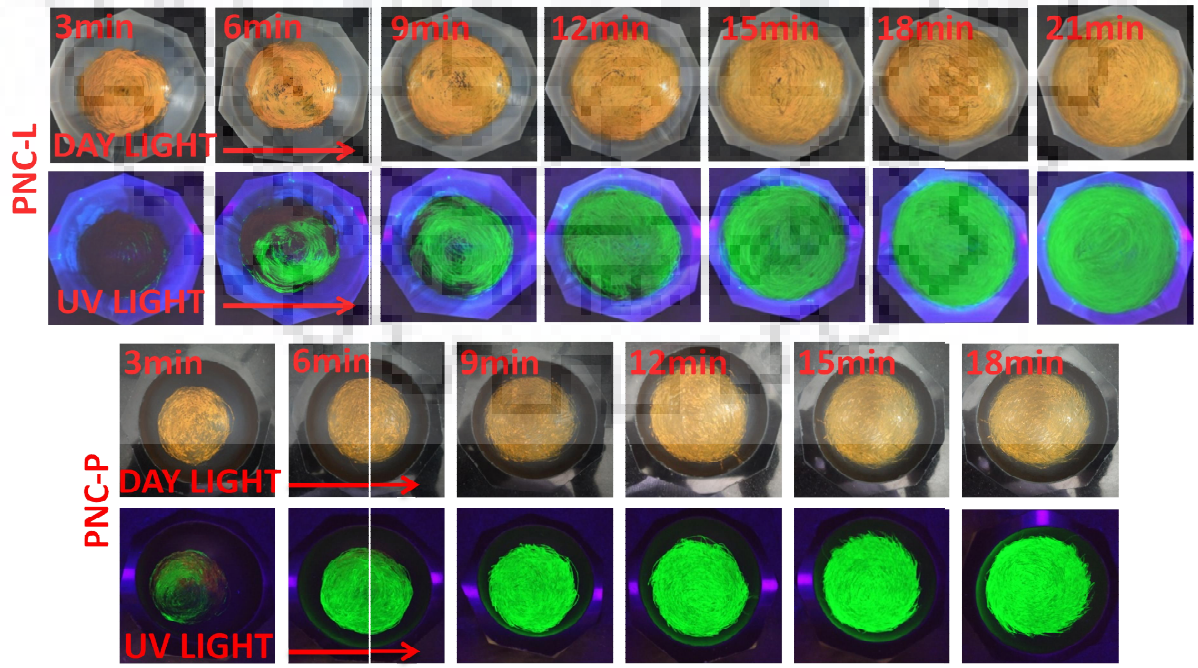

Figure 3.2.2.1: Grinding time dependent day light and corresponding UV light images of PNC-L and PNC-P at an interval of 3 minutes.

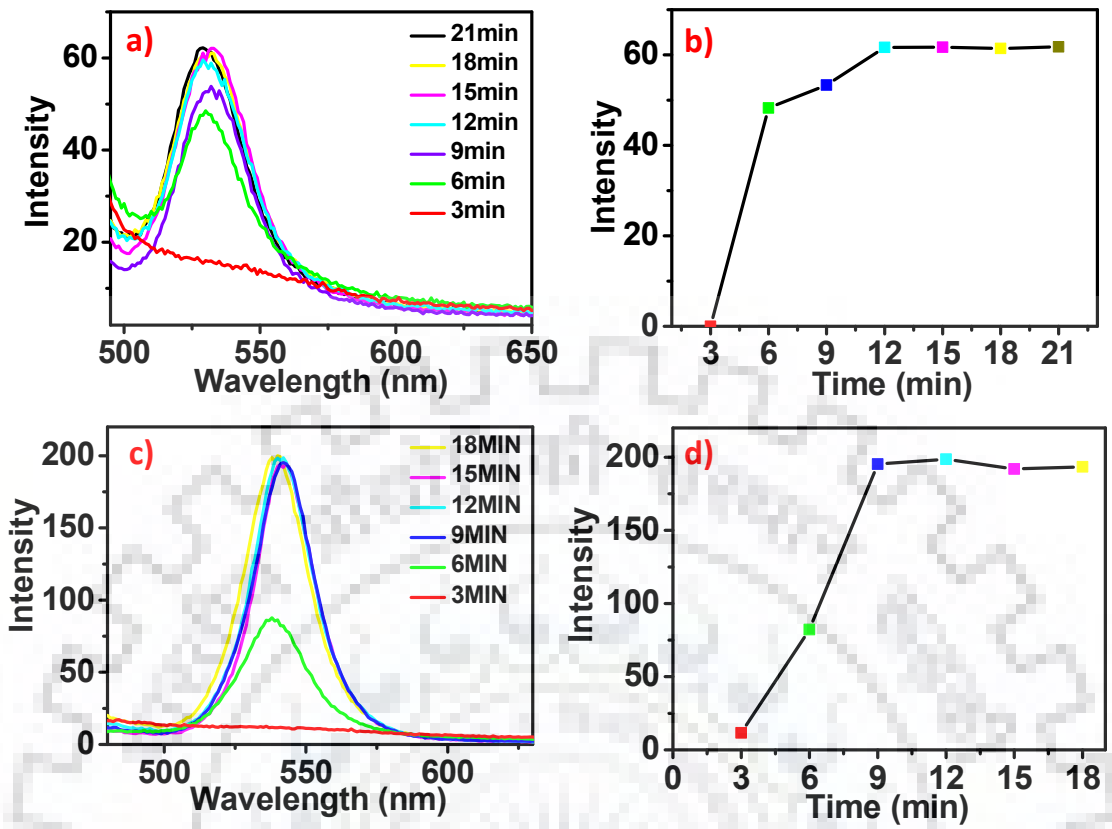

Figure 3.2.2.2: a) Photoluminescence (PL) spectra of PNC-L at different grinding time, b) PL intensity versus time (min) plot of PNC-L, c) Photoluminescence (PL) spectra of PNC-P at different grinding time, d) PL intensity versus time (min) plot of PNC-P.

3.2.3 UV-DRS spectra of $MAPbBr_3$ PNCs using amino acids

UV-DRS spectra was observed as by making $MAPbBr_3$ PNCs using different amino acid and dried $BaSO_4$ as reference. We have taken UV-DRS spectra of $MAPbBr_3$ PNCs using Glycine, Alanine, Leucine and Phenylalanine. UV-DRS studies have shown that PNC-G, PNC-A, PNC-L and PNC-P exhibited sharp band at 508.3 nm, 512.4 nm, 518 nm and 513.7 nm respectively, shown in Figure 3.2.3.1.

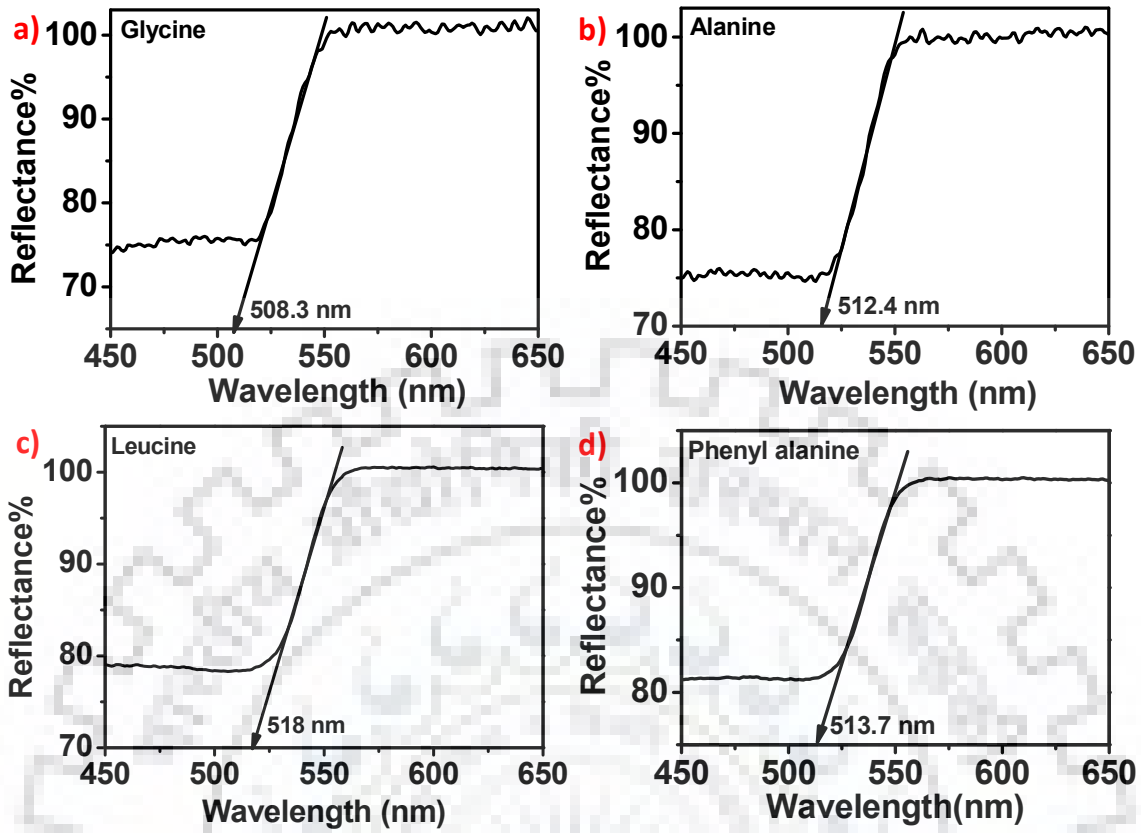

Figure 3.2.3.1: a) UV-DRS spectra of PNC-G, b) UV-DRS spectra of PNC-A, c) UV-DRS spectra of PNC-L, d) UV-DRS spectra of PNC-P.

3.2.4 Photoluminescence (PL) spectra of $MAPbBr_3$ PNCs using amino acids

At room temperature, we have investigated Glycine, Alanine, Leucine and Phenylalanine as bidentate ligand during synthesis of $MAPbBr_3$ PNCs by mechanochemical synthesis. Photoluminescence increase upon increasing the hindrance of capping ligand. We had found that out of Glycine, Alanine and Leucine (alkyl chain containing amino acids), containing $MAPbBr_3$ PNCs, Leucine containing $MAPbBr_3$ PNCs showed highest fluorescence intensity due to larger alkyl chain length. In comparison of PNC-L and PNC-P, PNC-P showed higher PL intensity due to higher hindrance of phenyl group. In PL spectrum, PNC-G and PNC-A had showed very negligible fluorescence. The green fluorescence PL intensity order was found to be PNC-G<PNC-A<PNC-L<PNC-P, shown in Figure 3.2.4.1. The PL emission band of PNC-G, PNC-A, PNC-L and PNC-P are shown at 526 nm, 530 nm, 540 nm and 542 nm respectively. Single PL emission peak in PL spectrum had shown the formation of uniform nanoparticles of $MAPbBr_3$ perovskite.

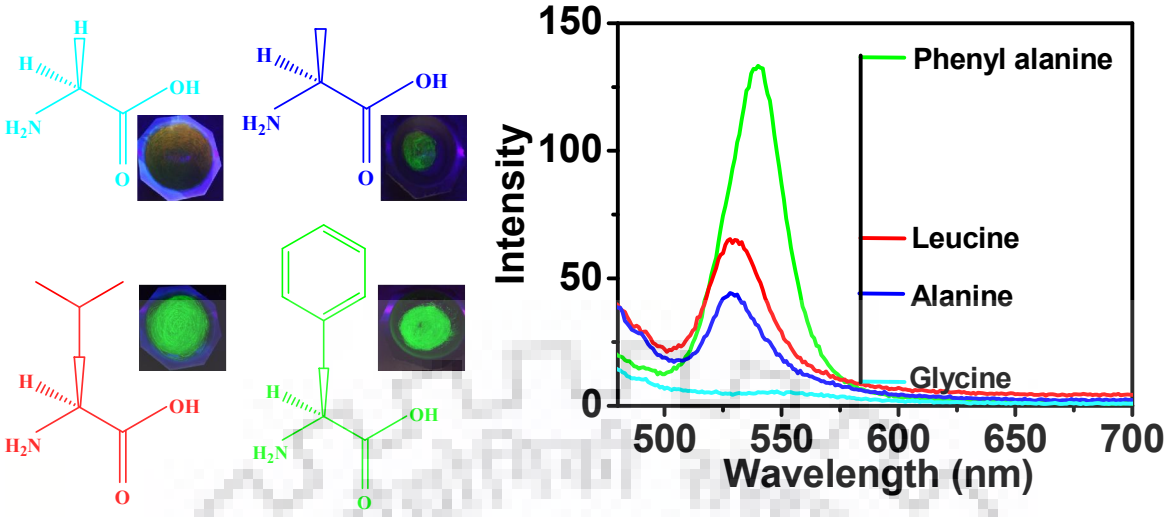

Figure 3.2.4.1: structure of Glycine, Alanine, Leucine, Phenylalanine along with PNCs images under UV light and PL spectra of $MAPbBr_3$ PNCs using amino acids.

3.2.5 Powder XRD of PNC-L and PNC-P

Morphological and structural studies have been done by TEM and XRD, respectively. The powder XRD pattern of PNC-L and PNC-P at optimized condition show cubic phase of $MAPbBr_3$ PNCs with *Pm-3m* space group. In Powder XRD pattern, peaks appear at 2θ values 15.08°, 21.40°, 26.18°, 30.24°, 33.93°, 37.28°, 43.25°, 45.99°, 48.62°, 53.63°, 55.89° and 58.28° corresponding to plane (001), (110), (111), (002), (021), (211), (220), (003), (310), (222), (023) and (123) respectively shown in Figure 3.2.5.1and parameter in Table 3.2.5.1. The highest intensity peak appear at 33.93 (2θ) value in PNC-L and PNC-P correspond to (021) plane. The plane (021), (023), (002) and (123) of powder XRD fully match with SAED pattern of TEM, that confirm the formation of cubic $MAPbBr_3$ PNCs.

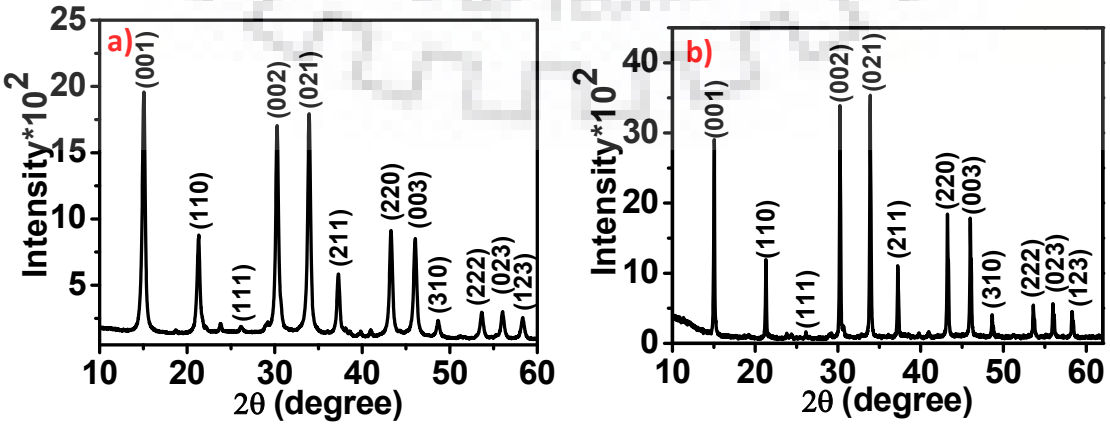

Figure 3.2.5.1: a) XRD pattern of PNC-L, b) XRD pattern of PNC-P.

Table 3.2.5.1: Powder XRD parameters of PNC-L.

2Θ	Θ	sinΘ	$Sin^2Θ$	Ratio	d	(hkl)
15.08	7.54	0.1312	0.0172	1	5.8848	(001)
21.40	10.70	0.1857	0.0344	2.00	4.1575	(110)
26.18	13.09	0.2264	0.0512	2.98	3.4095	(111)
30.24	15.12	0.2608	0.0680	3.95	2.9600	(002)
33.93	16.96	0.2917	0.0850	4.94	2.6464	(021)
37.28	18.64	0.3196	0.1021	5.93	2.4159	(211)
43.25	21.62	0.3685	0.1357	7.89	2.0953	(220)
45.99	22.99	0.3906	0.1525	8.87	1.9767	(003)
48.62	24.31	0.4116	0.1694	9.84	1.8757	(310)
53.63	26.81	0.4511	0.2034	11.83	1.7117	(222)
55.89	27.94	0.4685	0.2194	12.76	1.6480	(023)
58.28	29.14	0.4869	0.2370	13.78	1.5858	(123)

3.2.6 Fourier Transform Infrared (FTIR) Spectroscopy of PNC-L and PNC-P

Binding between $MAPbBr_3$ PNCs and capping ligand was confirmed by FTIR spectroscopy. We had studied infra-red spectra of Leucine, Phenylalanine, PNC-L and PNC-P. We have found that some peaks were disappeared in PNC-L and PNC-P due to binding of Leucine and Phenylalanine with $MAPbBr_3$ PNCs, shown in Figure 3.2.6.1. In FT-IR spectrum of PNC-L and PNC-P, IR bands were observed at (Figure 3.2.6.1) 2720 cm^{-1}, 2616 cm^{-1} and 2135 cm^{-1} are corresponding to combination band of NH_3^+. Some other bands 1605 cm^{-1} asymmetric bending of NH_3^+, 1576 cm^{-1} asymmetric stretching of COO^-, 1533 cm^{-1} symmetric deformation of NH_3^+, 1421 cm^{-1} stretching of CH_3, 1405 cm^{-1} symmetric stretching of COO^-, 1376 cm^{-1} CH_2 deformation, 1341 cm^{-1} CH_2 wagging motion and 1309 cm^{-1} symmetric bending of CH_3 were observed. PNC-L shown IR peak at 2969 cm^{-1} asymmetric stretching of CH_2.

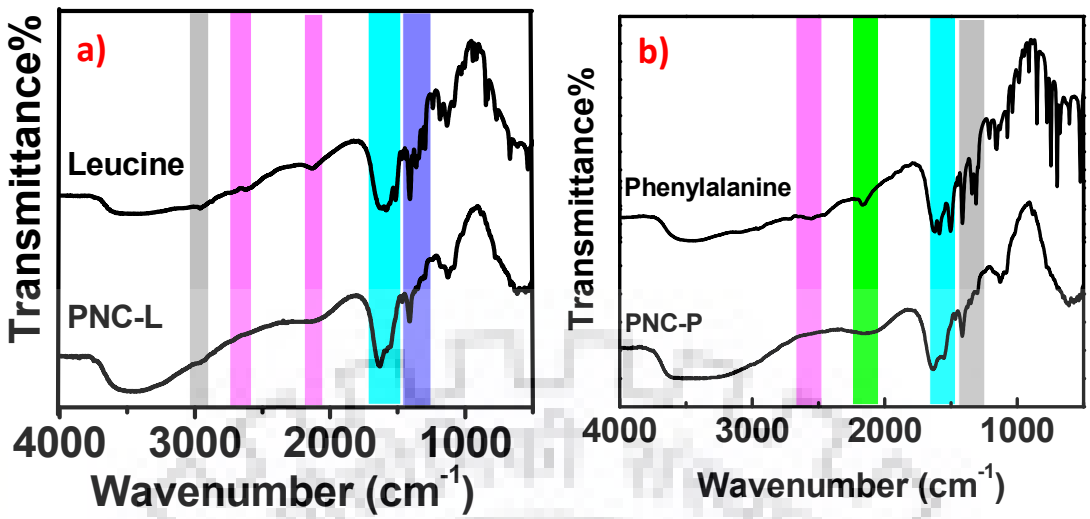

Figure 3.2.6.1: a) FTIR spectrum of Leucine and PNC-L, b) FTIR spectrum of Phenylalanine and PNC-P.

3.2.7 ^{1}H NMR and ^{13}C Solid NMR spectra of of Leucine-PNC-L.

Binding between surface of $MAPbBr_3$ PNCs and capping ligand amino acid was explained by ^{1}H NMR and ^{13}C Solid NMR spectra of Leucine as well as PNC-L. ^{1}H NMR spectra was shown in Figure 3.2.7.1, indicating multiplet at 0.88 ppm and singlet at 1.23 ppm which was corresponding to protons of ligand leucine. Whereas other two peaks at 2.37 ppm and 7.51 ppm was corresponding to methylammonium protons of $MAPbBr_3$ PNCs. We had also performed ^{13}C solid NMR of Leucine and $MAPbBr_3$ PNCs. We had observed four peaks in Leucine due to overlapping of two peaks and five peaks in PNC-L, because one extra peak coming from methylammonium carbon of $MAPbBr_3$. In Leucine, ^{13}C Solid NMR spectra peaks were appeared at 24.69 ppm (s), 41.6 ppm (d), 53.43 ppm (d) and 176.21 ppm (d). Whereas in PNC-L ^{13}C Solid NMR spectra peaks appear at 25.22 ppm (s), 30.85 ppm (s), 42.12 ppm (d), 54.15 ppm (d) and 176.8 ppm (d), shown in Figure 3.2.7.2.

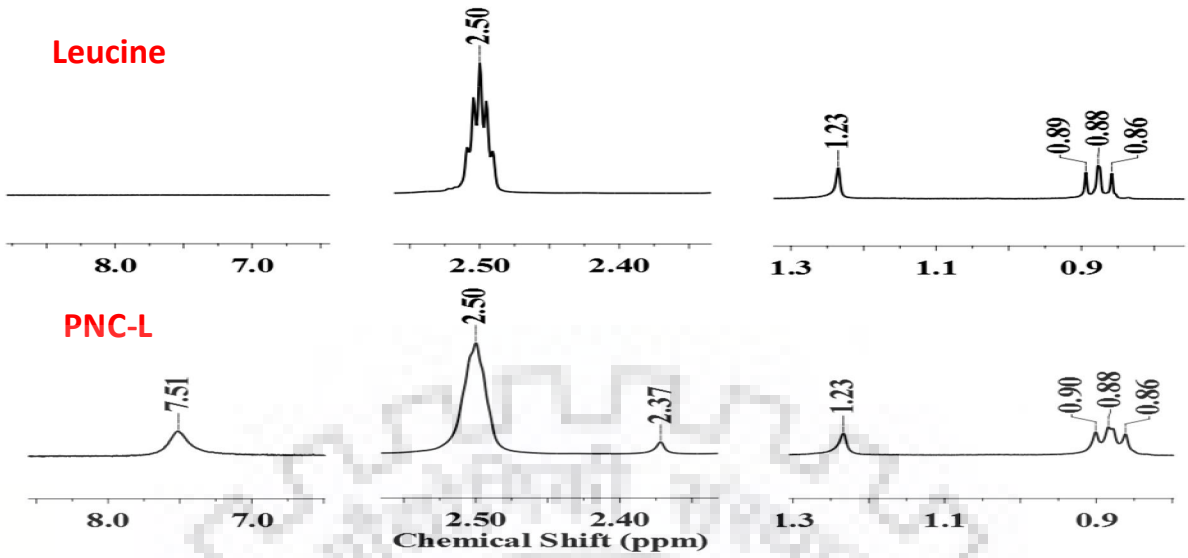

Figure 3.2.7.1: ^{1}H NMR spectra of Leucine and PNC-L.

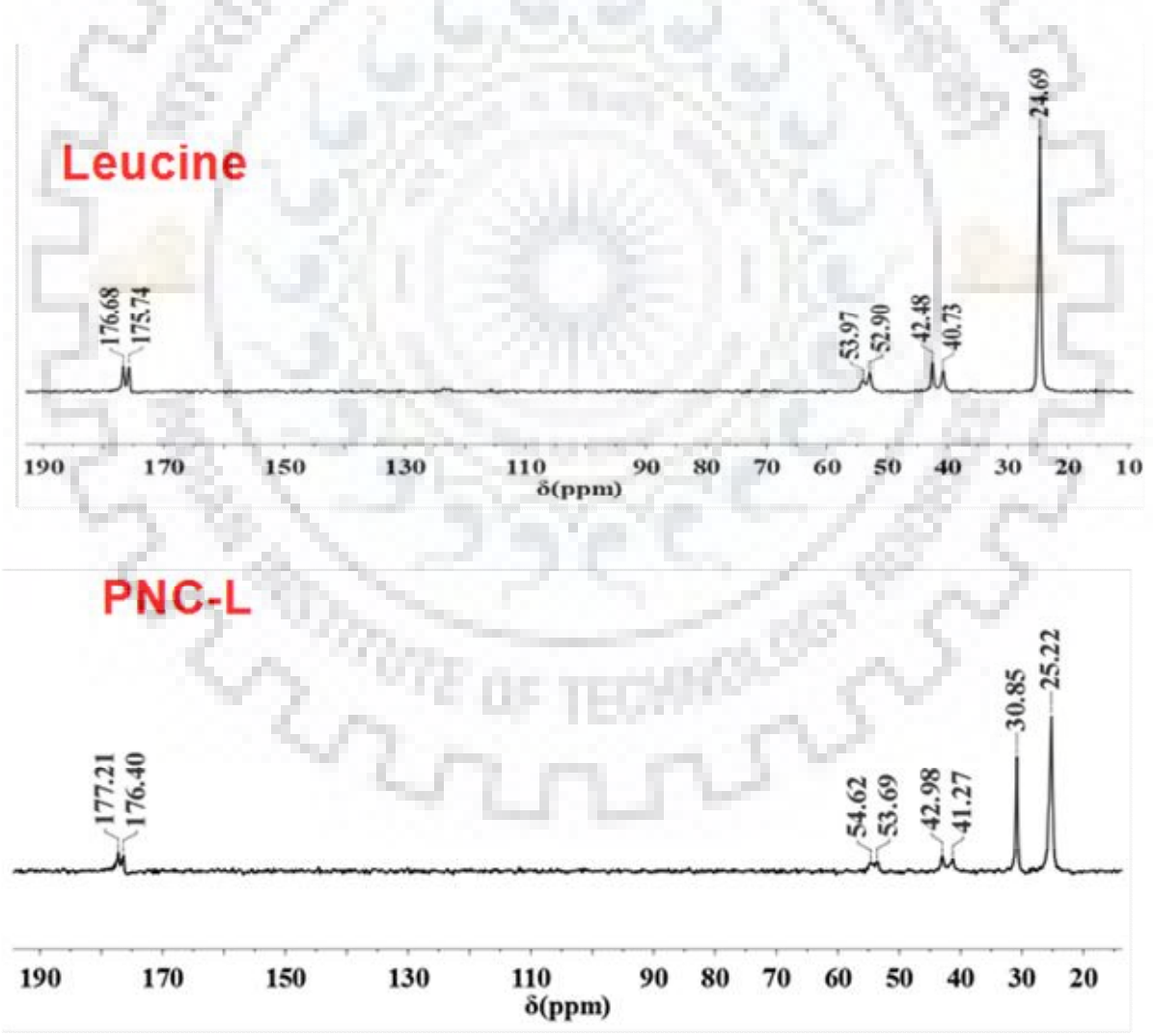

Figure 3.2.7.2: ^{13}C Solid NMR spectra of Leucine and PNC-L.

3.2.8 X-Ray Photoelectron Spectroscopy (XPS) analysis of PNC-L and PNC-P

The elemental ratio and composition of compound was characterized by X-Ray Photoelectron Spectroscopy. Full scan surface analysis as well as narrow scan of $MAPbBr_3$ PNCs, PNC-L and PNC-P are shown in Figure 3.2.8.1 and Figure 3.2.8.2. Lead 4f, carbon 1s, nitrogen 1s and bromide 3d peaks had confirmed the formation of $MAPbBr_3$ PNCs. In PNC-L, Lead 4f shown two major peaks at 137.29 eV and 142.15 eV, corresponding to Pb $4f_{7/2}$ and $4f_{5/2}$ respectively, along with small peaks at 135.16 eV and 140.07 eV. Whereas bromide 3d peaks are shown in between 67.11-68.11 eV, corresponding to $3d_{5/2}$ and $3d_{3/2}$. In PNC-P, Lead 4f had shown two major peaks at 137.79 eV and 142.75 eV corresponding to Pb $4f_{7/2}$ and $4f_{5/2}$ respectively, along with small peaks at 135.21 eV and 140.21 eV. Whereas Bromide 3d shown peak in between 67.21-68.85 eV corresponding to $3d_{5/2}$ and $3d_{3/2}$, carbon 1s at 284.76 eV and nitrogen 1s at 401.88 eV binding energy scale. Composition of element in PNC-L and PNC-P shown in Table 3.2.8.1 and 3.2.8.2 respectively.

Table 3.2.8.1: XPS composition data of PNC-L.

C1s	N1s	Br3d	Pb4f
89.35	0.00	7.94	2.71

Table 3.2.8.2: XPS composition data of PNC-P.

C1s	N1s	Br3d	Pb4f
69.72	2.66	2.07	1.17

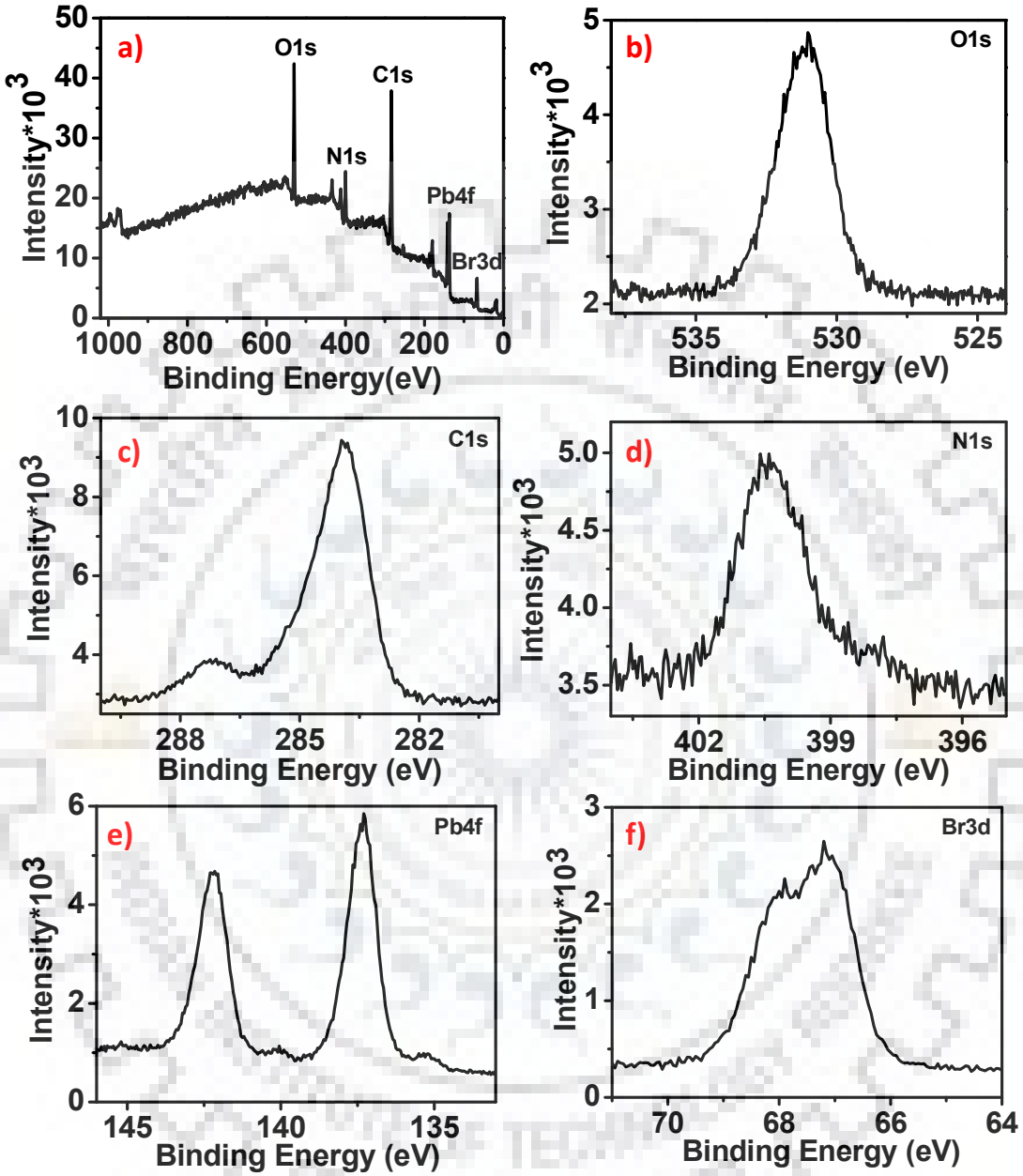

Figure 3.2.8.1: a) XPS survey scan of PNC-L, b) Narrow scan of O 1s, c) Narrow scan of C 1s, d) Narrow scan of N 1s, e) Narrow scan of Pb 4f, f) Narrow scan of Br 3d.

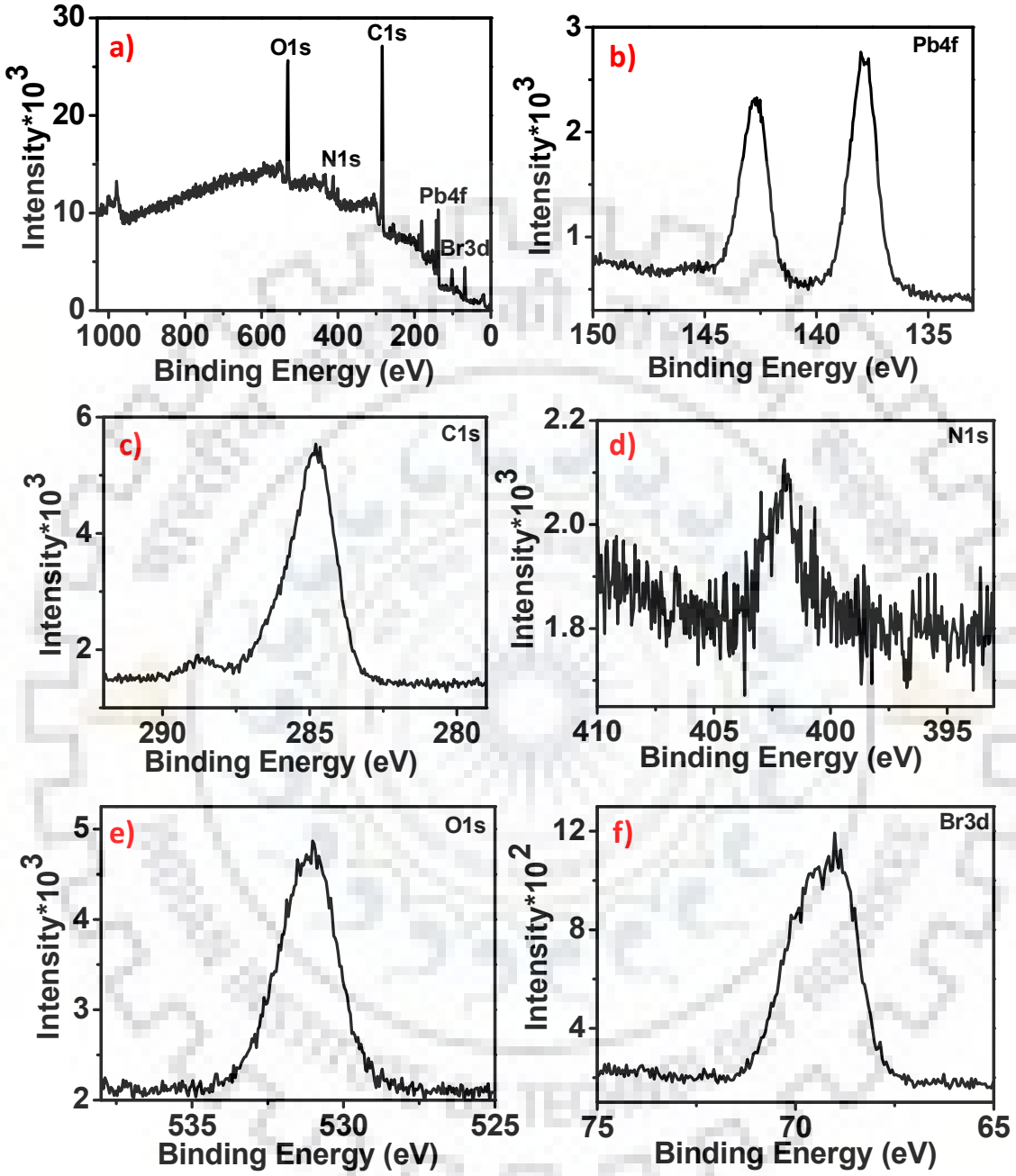

Figure 3.2.8.2. a) XPS survey scan of PNC-P, b) Narrow scan of Pb 4f, c) Narrow scan of C 1s, d) Narrow scan of N 1s, e) Narrow scan of O 1s, f) Narrow scan of Br 3d.

3.2.9 Time dependent stability of PNC-L by XRD and XPS

Additionally, with respect to stability of perovskite nanocrystals, XRD and XPS analysis has been performed as a function of time; no obvious reduction in the intensity of diffraction peaks is observed at different points of time. Moreover no peaks related to phase transition is found over 6 months of time as shown in Figure 3.2.9.1. This shows the importance of ligands towards high stability of perovskites over the perovskite synthesized using conventional ligands including oleic acid , oleylamine and octylamine.

Time dependent XPS studies have also confirmed the presence of all elements with no changes in their binding energy confirming the stability (Figure 3.2.9.1(a)) of these nanocrystals in ambient condition.

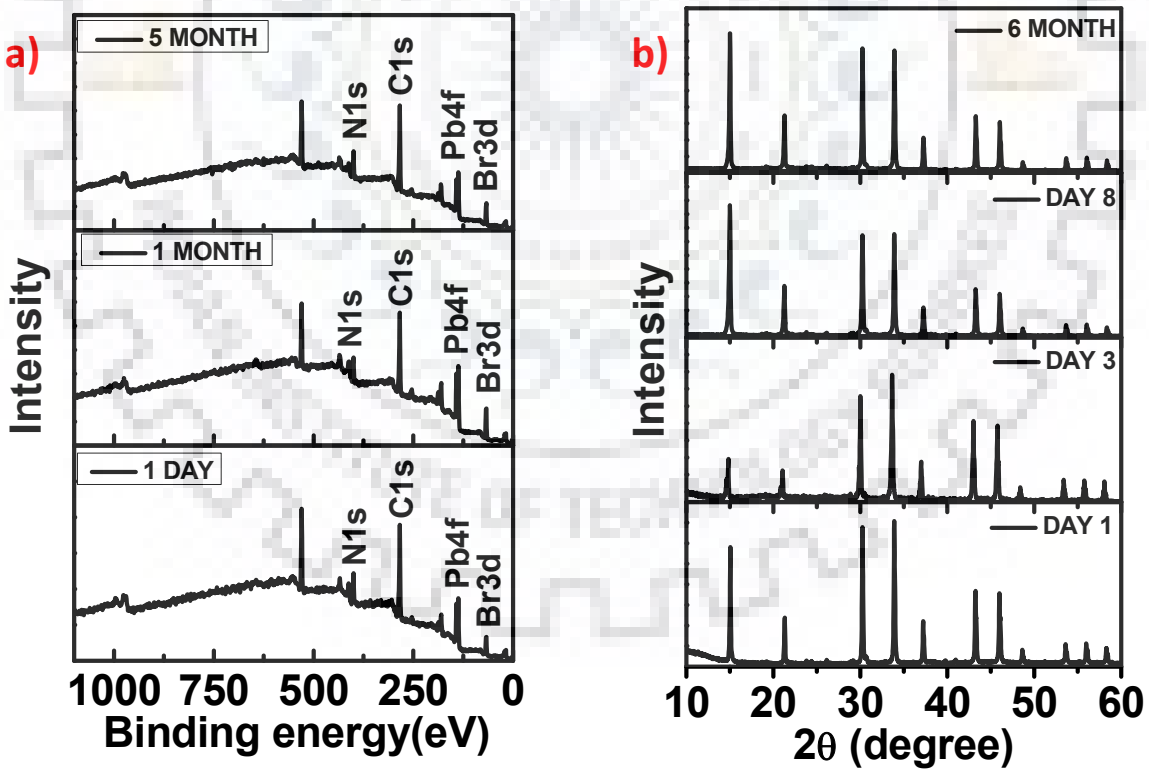

Figure 3.2.9.1: a) Time dependent XPS analysis of PNC-L, b) Time dependent XRD spectra of PNC-L.

3.2.10 Temperature dependent thermal stability of PNC-L and PNC-P

To demonstrate the stability of leucine and phenylalanine treated $MAPbBr_3$ nanocrystal, we have tracked the thermo-gravimetric analysis and temperature dependent PL studies. In Figure 3.2.10.1(a), significant analysis of temperature dependent studies of PNC-L have shown that it is stable upto around 100^0C with small changes in intensity. As depicted from Figure 3.2.10.1(a) emission band of $MAPbBr_3$ disappears at around 200^0C showing complete degradation of PNC-L. Also, Intensity vs. temperature graph has been shown in Figure 3.2.10.1(b) suggesting decrease of intensity of emission peak by increasing temperature. In Figure 3.2.10.2, DTA/TGA studies have shown the thermal decomposition of PNC-L. The first onset appears to decompose at 220^0C with weight loss of 18.6%, molecular weight calculated from curve is 113.4 which suggests the loss of organic material MABr. Second onset at 285^0C with weight loss of 15.8% is corresponding to the melting point of organic ligand used i.e. L-Leucine. The evolution of gases may be in the form of carbon dioxide, ammonia and small organic molecules. Third onset undergoes broad weight loss as seen in Figure 3.2.10.2(a) with app. weight loss of 62.4 % implies the inorganic material ie. $PbBr_2$. These results corroborates with the temperature dependent studies. TGA analysis of PNC-P is also mentioned in Figure 3.2.10.2(b).

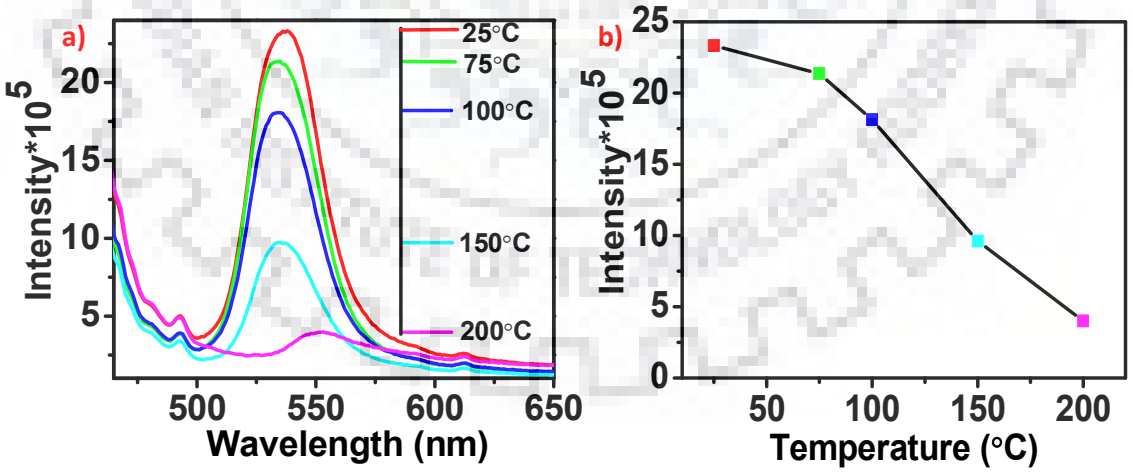

Figure 3.2.10.1: a) Temperature dependent PL spectra of PNC-L, b) PL intensity versus temperature (°C) graph of PNC-L.

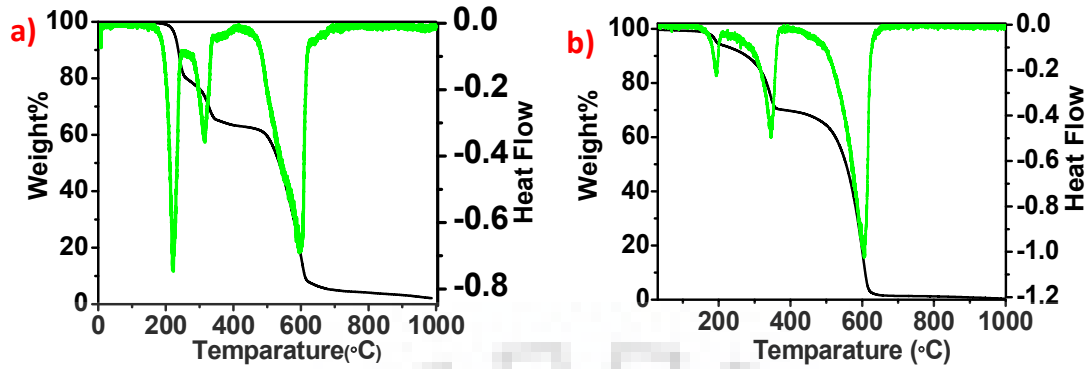

Figure 3.2.10.2: a) DTA-TGA curve of PNC-L, b) DTA-TGA curve of PNC-P.

3.2.11 Water stability analysis of PNC-L

Daylight as well as images under UV chamber of PNC-L after treatment with water are shown in Figure 3.2.11.1. In Figure 3.2.11.1, we have tried to investigate the stability of PNC-L in the presence of water. We have taken initial XRD pattern of PNC-L along with pure leucine. Later, we have added 5 ml of distilled water and dried it completely. Interestingly, it is observed that the X-ray diffraction peaks of perovskite structure are maintained after treatment with water and re-grinding, shown in Figure 3.2.11.3. PL studies of initial in addition to that after water treatment are shown in Figure 3.2.11.2. In general, hydrophobic ligands are used to maintain the stability of the nanocrystals. Use of the amino acid imparts an ambipolar nature which is responsible for the stability of these nanocrystals in ambient condition.

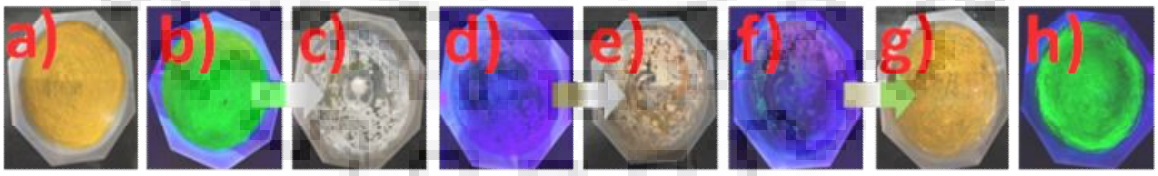

Figure 3.2.11.1: a) Daylight image of PNC-L after grinding at RT, b) Image of PNC-L (a) under UV chamber, c) Daylight image of PNC-L after adding 5 ml of water, d) Image of PNC-L (c) under UV chamber after adding 5 ml water, e) Daylight Image of PNC-L after getting it dried at RT as well as light heating, f) Image of PNC-L (e) under UV chamber after getting it dried at RT as well as light heating, g) Daylight image of PNC-L after grinding of dried perovskite, h) Image of grinded powder (g) after water treatment under UV chamber.

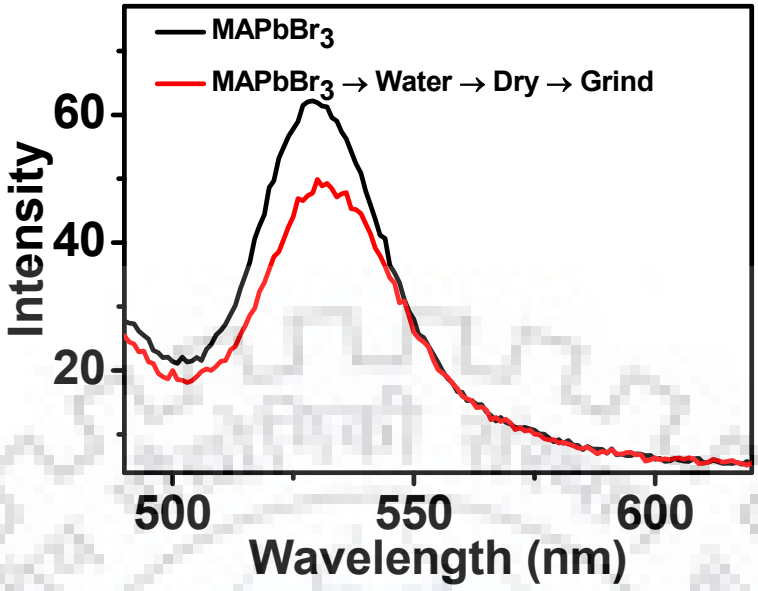

Figure 3.2.11.2: PL spectra of PNC-L after grinding of dried perovskite.

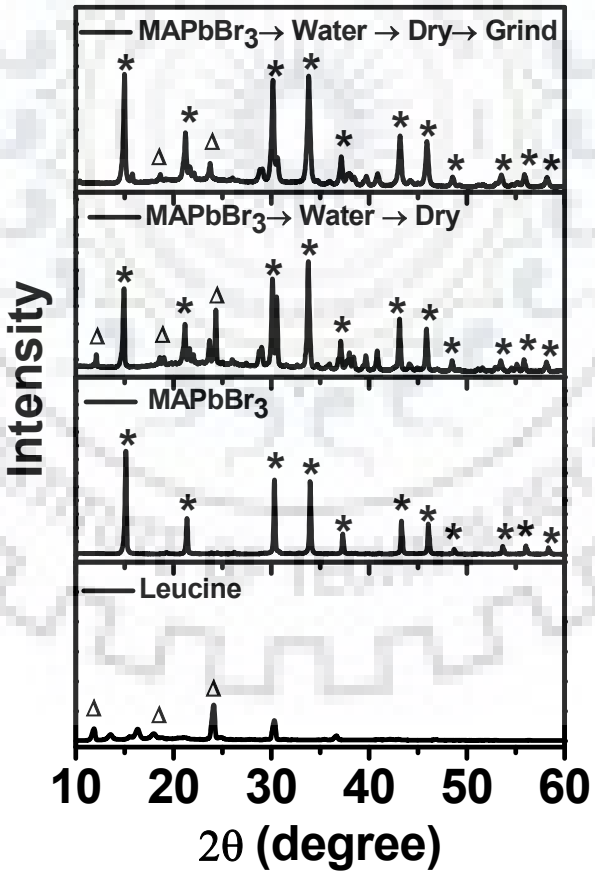

Figure 3.2.11.3: PNC-L analysis followed with steps of water 5 ml, dry and again grinding. Leucine XRD spectra with followed steps of PNC-L.

3.2.12 Morphological study of PNC-L and PNC-P

3.2.12.1 Atomic Force Microscopy (AFM)

Surface analysis of PNC-L was carried out by Atomic Force Microscopy (AFM). Generally, Three techniques were used for morphological studies, 1) Atomic Force Microscopy, 2) Scanning Electron Microscopy, and 3) Transmission Electron Microscopy. AFM images of PNC-L shown 2D and 3D suface morphology, Which shown in Figure 3.2.12.1.1.

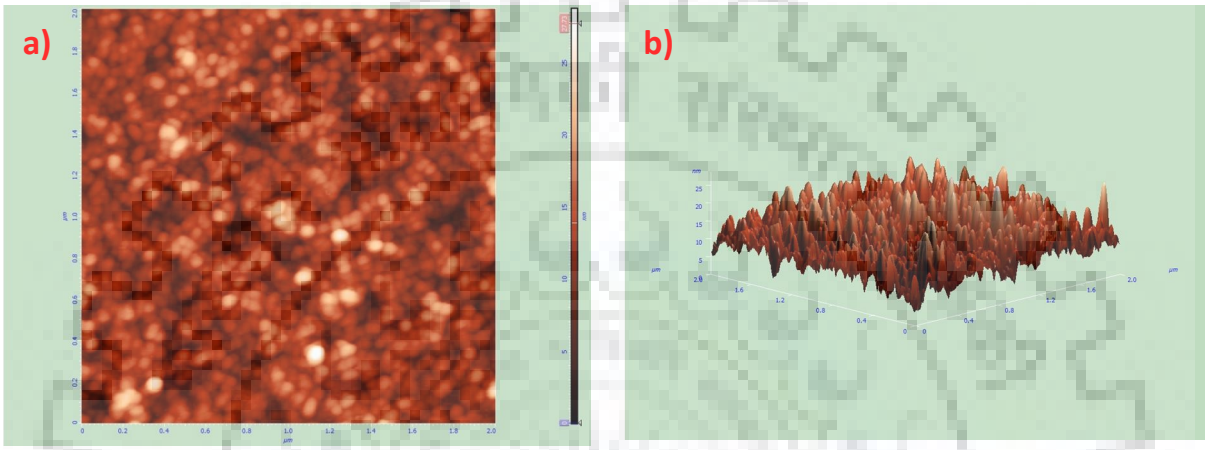

Figure 3.2.12.1.1: a) AFM 2D image of PNC-L, b) AFM 3D image of PNC-L.

3.2.12.2 Scanning Electron Microscopy (SEM)

Morphological studies of PNC-L and PNC-P were carried out by Scanning Electron Microscopy (SEM) and small spherical morphology was obtained, which shown in Figure 3.2.12.2.1. We have performed SEM EDX analysis of PNC-L and PNC-P, shown in Figure 3.2.12.2.2 and 3.2.12.2.3. SEM EDX composition analysis of PNC-L confirmed the elemental composition of Pb and Br in 1 : 3.27 shown in Table 3.2.12.2.1. This ratio was very close to ideal ratio 1 : 3. We also performed mapping of PNC-L to confirmed the elemental presence, shown in Figure 3.2.12.2.4.

Table 3.2.12.2.1: SEM EDX composition analysis of PNC-L.

Element	Weight%	Atomic%
C K	15.04	62.27
Br L	47.45	29.53
Pb M	37.65	9.04

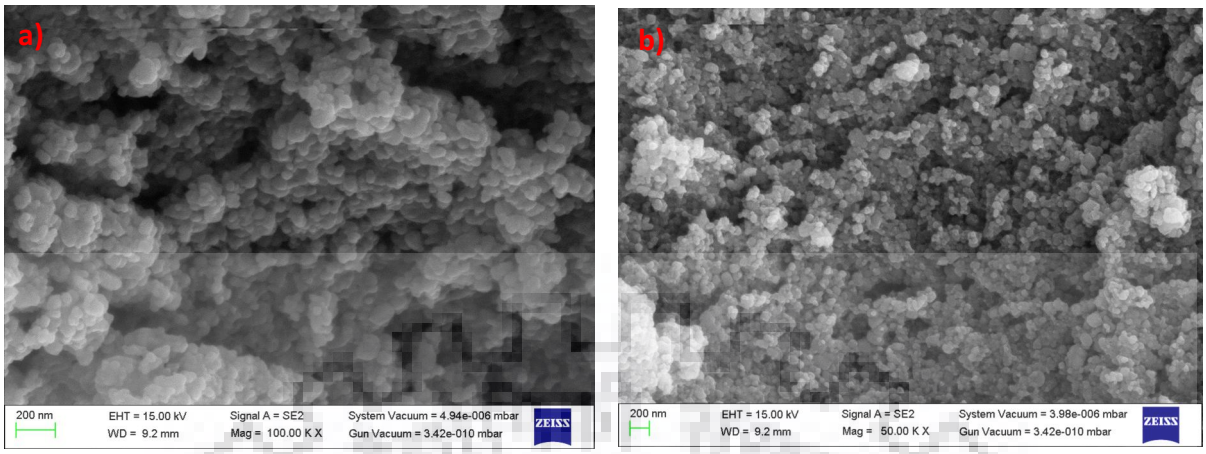

Figure 3.2.12.2.1: a) SEM image of PNC-L at 200 nm scale, b) SEM image of PNC-P at 200 nm scale.

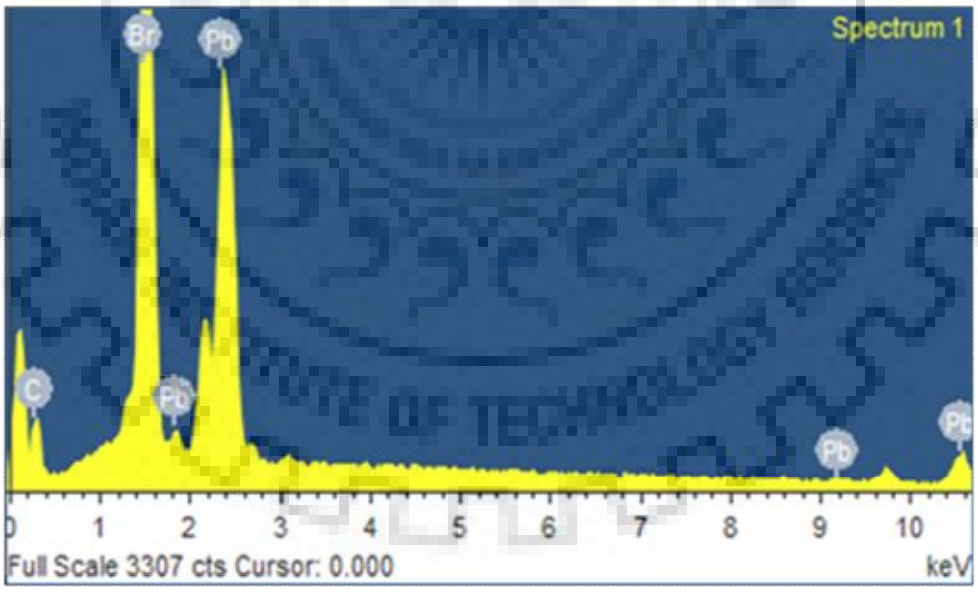

Figure 3.2.12.2.2: SEM EDX analysis of PNC-L.

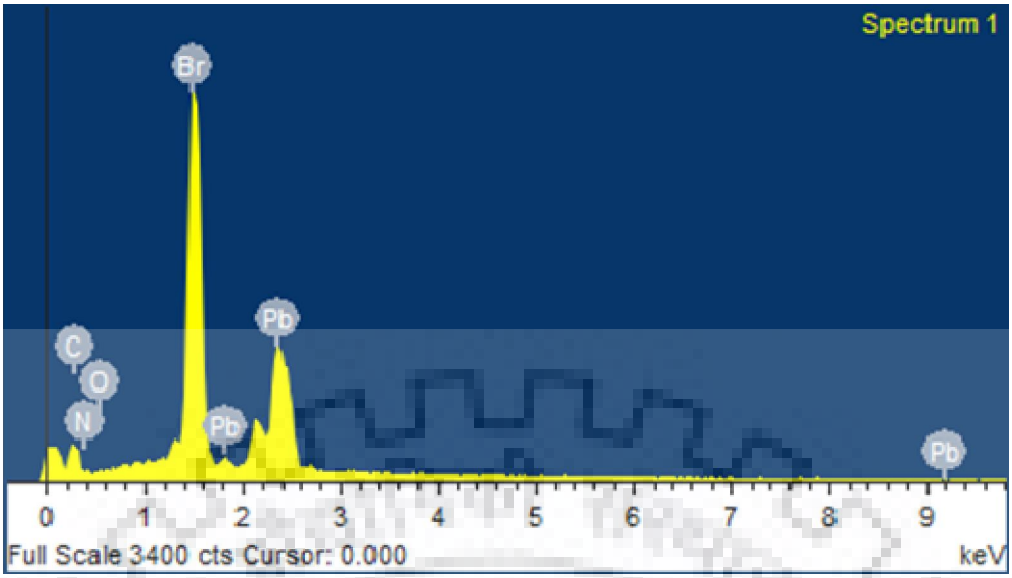

Figure 3.2.12.2.3: SEM EDX analysis of PNC-P.

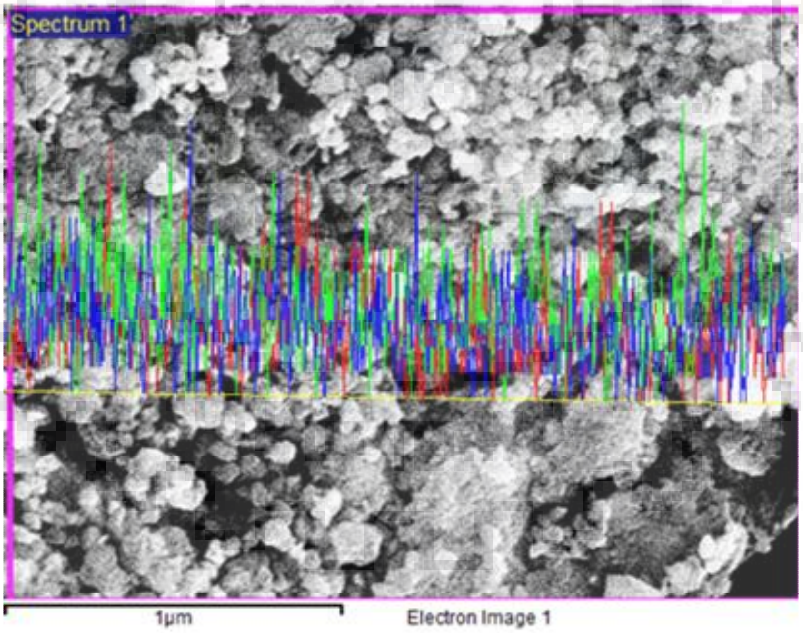

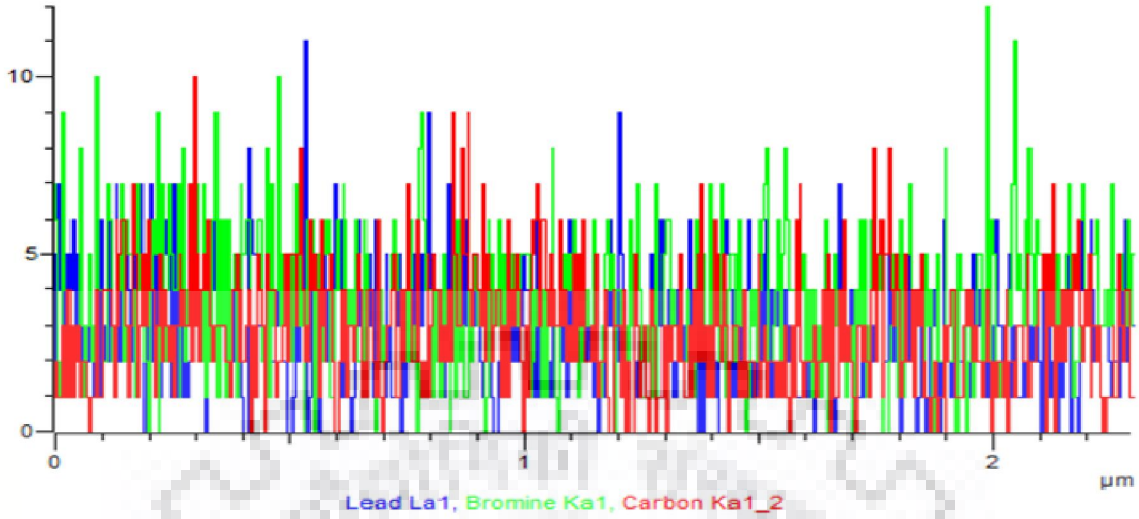
10
5
0
0
1
2
µm
Lead La1, Bromine Ka1, Carbon Ka1_2

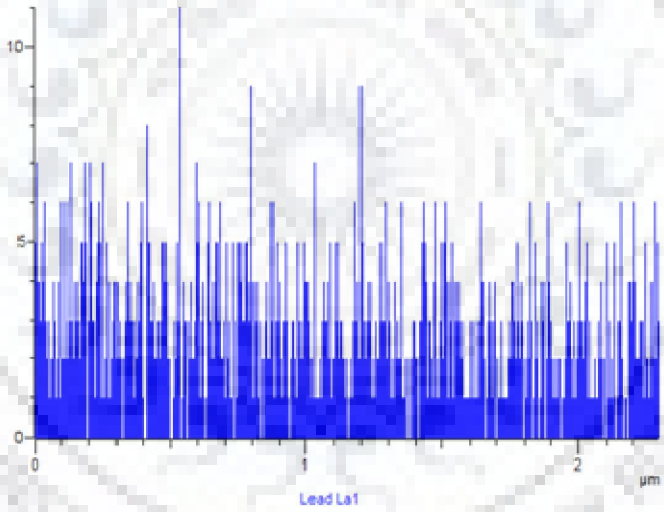
10
5
0
0
1
2
µm
Lead La1

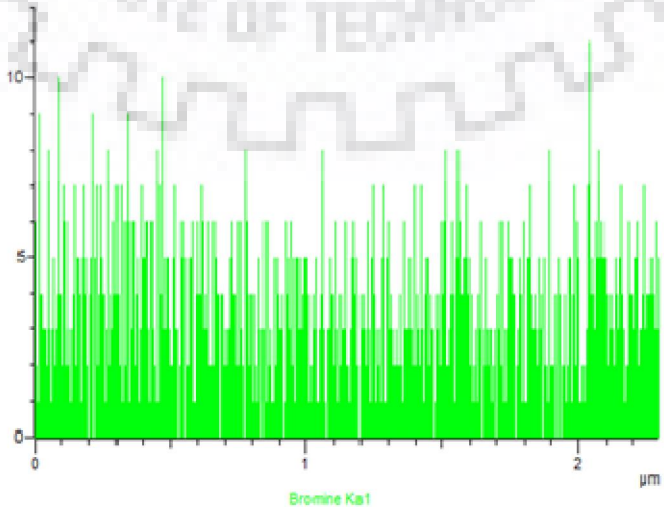
10
5
0
0
1
2
µm
Bromine Ka1

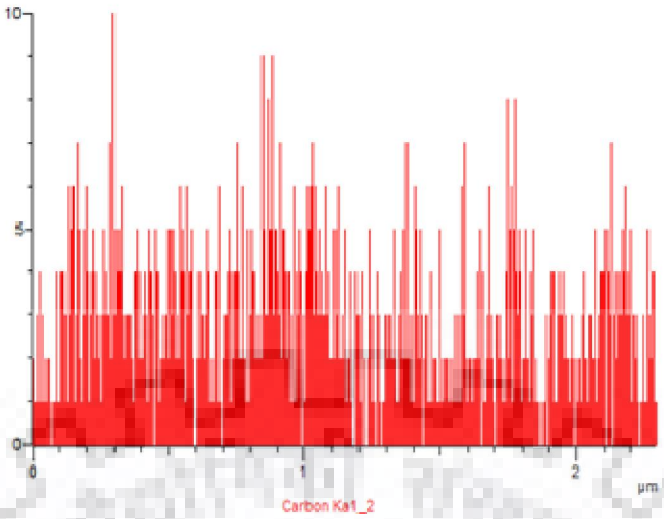

Figure 3.2.12.2.4: SEM maping analysis of PNC-L.

3.2.12.3 Transmission Electron Microscopy (TEM)

These perovskite materials are highly sensitive towards electron beam of TEM. TEM images of PNC-L at scale bar of 200 nm, 100 nm and 50 nm reveals the average size of quantum dots to be 3.5 nm, as shown in Figure 3.2.12.3.1. Also, Selected Area Electron Diffraction (SAED) pattern of PNC-L in Figure 3.2.12.3.3 shows the presence of planes (002), (021), (023) and (123) along with value of interplanar distance as $d_{(002)}$=2.960±0.1 Å, $d_{(021)}$= 2.646±0.07 Å, $d_{(023)}$= 1.672±0.02 Å and $d_{(123)}$= 1.585±0.05 Å, suggesting crystallinity of quantum dots is matching well with XRD pattern. EDX analysis is also shown in Figure 3.2.12.3.2 confirming the presence of all elements.

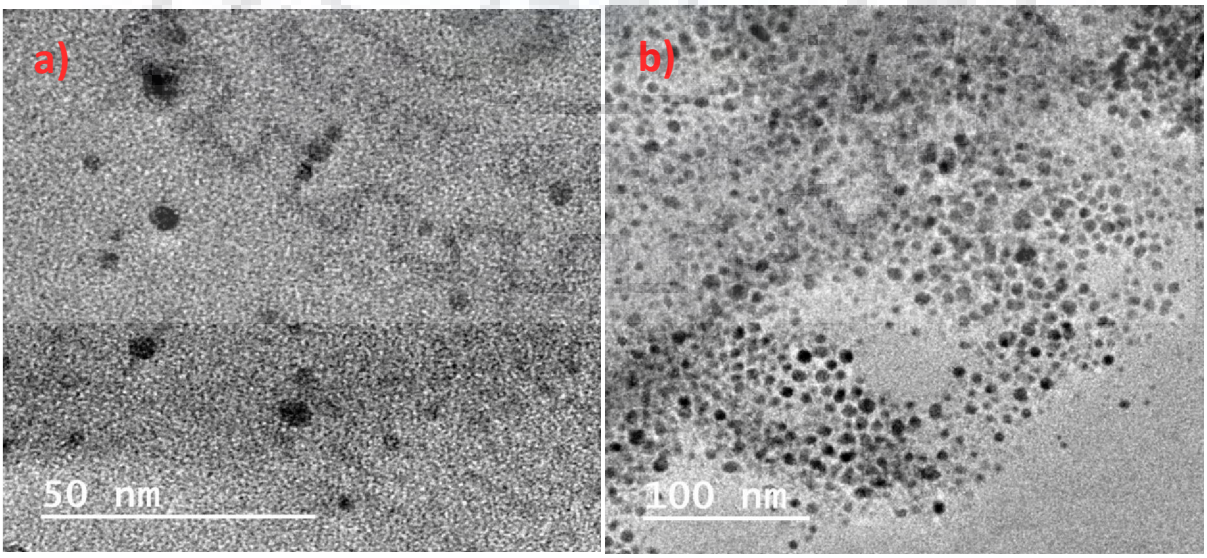

Figure 3.2.12.3.1: a) and b) TEM images of PNC-L at 50nm and 100 nm scale bar.

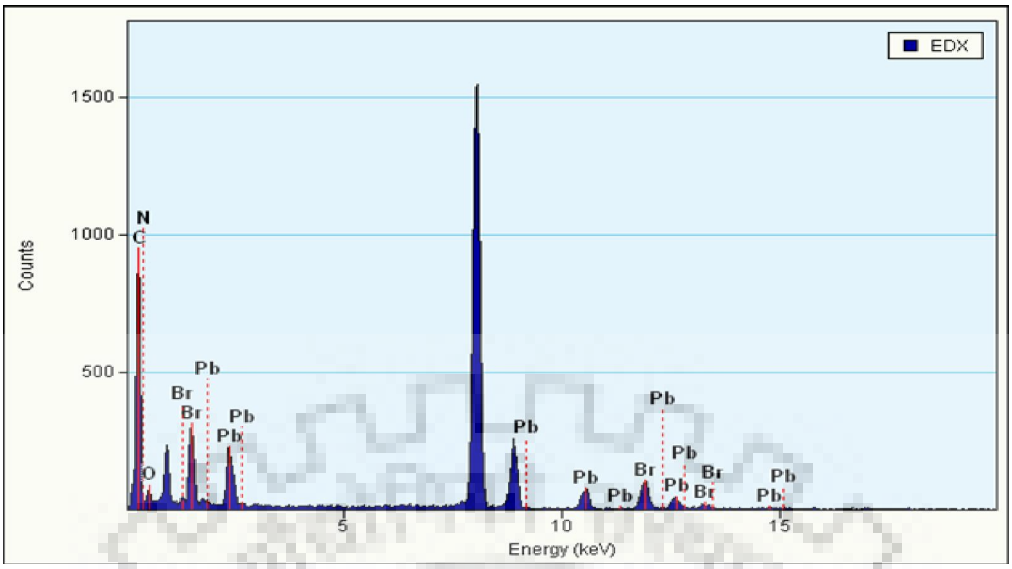

Figure 3.2.12.3.2: TEM-EDX image of PNC-L.

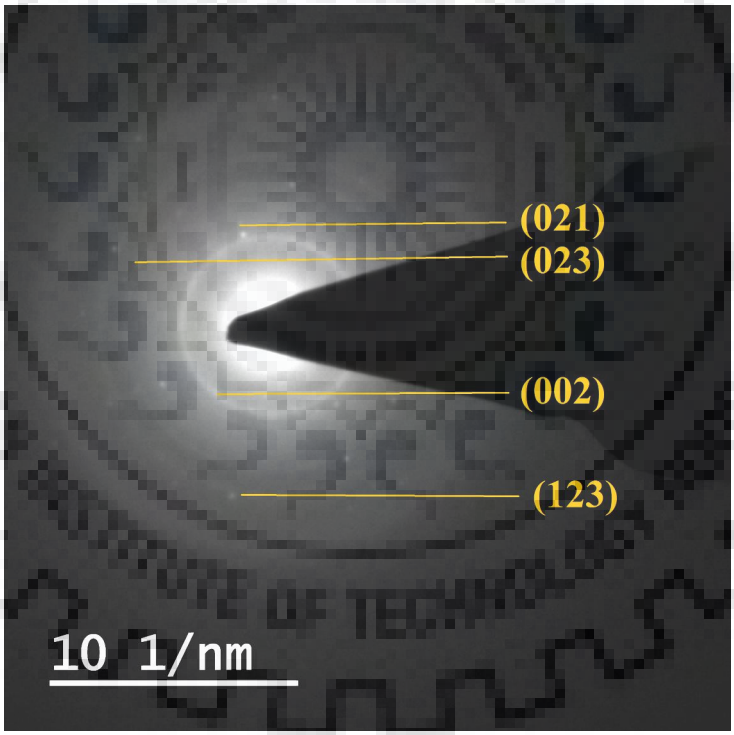

Figure 3.2.12.3.3: TEM-SAED pattern of PNC-L.

CONCLUSIONS

In summary, we have developed new approach towards ravelling of new non-toxic ligands over conventional ligands. The advantage of the use of amino acids as ligand is the presence of zwitterionic bi-functional moities in a single molecular species. A series of amino acids are tested and it is found that Phenyl alanine and leucine are most promising for the fluorescent solid solution. In presence of all precursors on the surface of flexible conducting plate, simple scratching is sufficient for the formation of ordered fluorescent nanocrystals. These nanocrystals are stable in ambient conditions for a long time.

Future Scope:

METHOD	PEROVSKITE	LIGANDS	RESULT
Mechanochemical	$MAPbBr_3$	Coconut Oil + Oleylamine	fluorescent

METHOD	PEROVSKITE	LIGANDS
Solvent free	Pb free	Waste material

REFERENCES

1. Zhu J., Thomas A., Perovskite-type mixed oxides as catalytic material for NO removal. *Appl. Catal. B- Environ.* **2009,** *92* (3-4), 225-233.

2. Goldschmidt V. M., Die gesetze der krystallochemie. *Naturwissenschaften* **1926,** *14* (21), 477-485.

3. Tejuca L. G., Fierro J. L., Properties and applications of perovskite-type oxides. *CRC Press*: **1992**.

4. Marcus Y., Thermodynamics of solvation of ions. Part 5. Gibbs free energy of hydration at 298.15 K. *J. Chem. Soc., Faraday Trans.* **1991,** *87* (18), 2995-2999.

5. Smith M. D., Connor B. A., Karunadasa H. I., Tuning the Luminescence of Layered Halide Perovskites. *Chem. rev.* **2019,** *119* (5), 3104-3139.

6. Huang H., Polavarapu L., Sichert J. A., Susha A. S., Urban A. S., Rogach A. L., Colloidal lead halide perovskite nanocrystals: synthesis, optical properties and applications. *NPG Asia Materials.* DOI:10.1038/am.2016.167.

7. Lin Q., Armin A., Nagiri R. C. R., Burn P. L., Meredith P., Electro-optics of perovskite solar cells. *Nat. Photonics* **2015,** *9* (2), 106-112.

8. Fu Y., Zhu H., Schrader A. W., Liang D., Ding Q., Joshi P., Hwang L., Zhu X., Jin S., Nanowire lasers of formamidinium lead halide perovskites and their stabilized alloys with improved stability. *Nano lett.* **2016,** *16* (2), 1000-1008.

9. Yao J. S., Ge J., Han B.-N., Wang K. H., Yao H.-B., Yu H. L., Li J. H., Zhu B. S., Song J. Z., Chen C., Ce^{3+} doping to modulate photoluminescence kinetics for efficient $CsPbBr_3$ nanocrystals based light-emitting diodes. *J. Am. Chem. Soc.* **2018,** *140* (10), 3626-3634.

10. Tong X. W., Kong W. Y., Wang Y. Y., Zhu J. M., Luo L. B., Wang Z. H., High-performance red-light photodetector based on lead-free bismuth halide perovskite film. *ACS appl. mater. interfaces* **2017,** *9* (22), 18977-18985.

11. Jodlowski A. D., Yépez A., Luque R., Camacho L., de Miguel G., Benign by Design Solventless Mechanochemical Synthesis of Three, Two, and One Dimensional Hybrid Perovskites. *Angew. Chem., Int. Ed.* **2016,** *55* (48), 14972-14977.

12. Zhu F., Men L., Guo Y., Zhu Q., Bhattacharjee U., Goodwin P. M., Petrich J. W., Smith E. A., Vela J., Shape evolution and single particle luminescence of organometal halide perovskite nanocrystals. *ACS nano* **2015,** *9* (3), 2948-2959.

13. Kim Y., Yassitepe E., Voznyy O., Comin R., Walters G., Gong X., Kanjanaboos P., Nogueira A. F., Sargent E. H., Efficient luminescence from perovskite quantum dot solids. *ACS appl. mater. & interfaces* **2015,** *7* (45), 25007-25013.

14. Saidaminov M. I., Abdelhady A. L., Maculan G., Bakr O. M., Retrograde solubility of formamidinium and methylammonium lead halide perovskites enabling rapid single crystal growth. *Chem. commun.* **2015,** *51* (100), 17658-17661.

15. Bansal P., Kar P., Ultralong Micro-belts of Luminescent Lead Halide based Perovskites. DOI:10.1039/c9cc02668a.

16. Yang D., Li X., Zeng H., Surface chemistry of all inorganic halide perovskite nanocrystals: passivation mechanism and stability. *Adv. Mater. Interfaces* **2018,** *5* (8), 1701662.

17. Ekimov A., Onushchenko A., Size quantization of the electron energy spectrum in a microscopic semiconductor crystal. *Jetp Lett* **1984,** *40* (8), 1136-1139.

18. Ashoori R., Electrons in artificial atoms. *Nature* **1996,** *379* (6564), 413-419.

19. Sichert J. A., Tong Y., Mutz N., Vollmer M., Fischer S., Milowska K. Z., García Cortadella R., Nickel B., Cardenas Daw C., Stolarczyk J. K., Quantum size effect in organometal halide perovskite nanoplatelets. *Nano lett.* **2015,** *15* (10), 6521-6527.

20. Zhang F., Zhong H., Chen C., Wu X., Hu X., Huang H., Han J., Zou B., Dong Y., Brightly luminescent and color-tunable colloidal $CH_3NH_3PbX_3$ (X= Br, I, Cl) quantum dots: potential alternatives for display technology. *ACS nano* **2015,** *9* (4), 4533-4542.

21. Protesescu L., Yakunin S., Bodnarchuk M. I., Krieg F., Caputo R., Hendon C. H., Yang R. X., Walsh A., Kovalenko M. V., Nanocrystals of cesium lead halide perovskites

($CsPbX_3$, X= Cl, Br, and I): novel optoelectronic materials showing bright emission with wide color gamut. *Nano lett.* **2015,** *15* (6), 3692-3696.

22. Jana A., Mittal M., Singla A., Sapra S., Solvent-free, mechanochemical syntheses of bulk trihalide perovskites and their nanoparticles. *Chem. Commun.* **2017,** *53* (21), 3046-3049.

23. Zheng L., Zhang D., Ma Y., Lu Z., Chen Z., Wang S., Xiao L., Gong Q., Morphology control of the perovskite films for efficient solar cells. *Dalton Trans.* **2015,** *44* (23), 10582-10593.

24. Burschka J., Pellet N., Moon S. J., Humphry Baker R., Gao P., Nazeeruddin M. K., Grätzel M., Sequential deposition as a route to high-performance perovskite-sensitized solar cells. *Nature* **2013,** *499* (7458), 316-319.

25. Levchuk I., Herre P., Brandl M., Osvet A., Hock R., Peukert W., Schweizer P., Spiecker E., Batentschuk M., Brabec C. J., Ligand-assisted thickness tailoring of highly luminescent colloidal $CH_3NH_3PbX_3$ (X= Br and I) perovskite nanoplatelets. *Chem. Commun.* **2017,** *53* (1), 244-247.

26. Sun S., Yuan D., Xu Y., Wang A., Deng Z., Ligand-mediated synthesis of shape-controlled cesium lead halide perovskite nanocrystals via reprecipitation process at room temperature. *ACS nano* **2016,** *10* (3), 3648-3657.

27. Pan J., Shang Y., Yin J., De Bastiani M., Peng W., Dursun I., Sinatra L., El Zohry A. M., Hedhili M. N., Emwas A. H., Bidentate ligand-passivated $CsPbI_3$ perovskite nanocrystals for stable near-unity photoluminescence quantum yield and efficient red light-emitting diodes. *J. Am. Chem. Soc.* **2017,** *140* (2), 562-565.

28. Luo B., Pu Y. C., Lindley S. A., Yang Y., Lu L., Li Y., Li X., Zhang J. Z., Organolead halide perovskite nanocrystals: branched capping ligands control crystal size and stability. *Angew. Chem., Int. Ed.* **2016,** *55* (31), 8864-8868.

29. Zhao J., Cao S., Li Z., Ma N., Amino Acid-Mediated Synthesis of $CsPbBr_3$ Perovskite Nanoplatelets with Tunable Thickness and Optical Properties. *Chem. Mater.* **2018,** *30* (19), 6737-6743.

30. Huang H., Susha A. S., Kershaw S. V., Hung T. F., Rogach A. L., Control of emission color of high quantum yield $CH_3NH_3PbBr_3$ perovskite quantum dots by precipitation temperature. *Adv. sci.* **2015,** *2* (9), 1500194-150098.

31. Wong A. B., Lai M., Eaton S. W., Yu Y., Lin E., Dou L., Fu A., Yang P., Growth and anion exchange conversion of $CH_3NH_3PbX_3$ nanorod arrays for light-emitting diodes. *Nano lett.* **2015,** *15* (8), 5519-5524.

32. Im J. H., Luo J., Franckevičius M., Pellet N., Gao P., Moehl T., Zakeeruddin, S. M., Nazeeruddin M. K., Grätzel M., Park N. G., Nanowire perovskite solar cell. *Nano lett.* **2015,** *15* (3), 2120-2126.

33. Bekenstein Y., Koscher B. A., Eaton S. W., Yang P., Alivisatos A. P., Highly luminescent colloidal nanoplates of perovskite cesium lead halide and their oriented assemblies. *J. Am. Chem. Soc.* **2015,** *137* (51), 16008-16011.

34. Liu J, Xue Y., Wang Z., Xu Z. Q., Zheng C., Weber B., Song J., Wang Y., Lu Y., Zhang Y., Bao Q., Two-dimensional $CH_3NH_3PbI_3$ perovskite: Synthesis and optoelectronic application. *ACS nano* **2016,** *10* (3), 3536-3542.

35. Wang C., Ecker B. R., Wei H., Huang J., Gao Y., Environmental surface stability of the $MAPbBr_3$ single crystal. *J. Phys. Chem. C* **2018,** *122* (6), 3513-3522.

36. Rajamanickam N., Kumari S., Vendra V. K., Lavery B. W., Spurgeon J., Druffel T., Sunkara M. K., Stable and durable $CH_3NH_3PbI_3$ perovskite solar cells at ambient conditions. *Nanotechnology* **2016,** *27* (23), 235404-235416.

37. Kojima A., Teshima K., Shirai Y., Miyasaka T., Organometal halide perovskites as visible-light sensitizers for photovoltaic cells. *J. Am. Chem. Soc.* **2009,** *131* (17), 6050-6051.

38. Yang W. S., Park B. W., Jung E. H., Jeon N. J., Kim Y. C., Lee D. U., Shin S. S., Seo J., Kim E. K., Noh J. H., Iodide management in formamidinium-lead-halide–based perovskite layers for efficient solar cells. *Science* **2017,** *356* (6345), 1376-1379.

39. DeQuilettes D. W., Koch S., Burke S., Paranji R. K., Shropshire A. J., Ziffer M. E., Ginger D. S., Photoluminescence lifetimes exceeding 8 μs and quantum yields exceeding

30% in hybrid perovskite thin films by ligand passivation. *ACS Energy Lett.* **2016,** *1* (2), 438-444.

40. Pan A., He B., Fan X., Liu Z. Urban J. J., Alivisatos A. P. He L., Liu Y., Insight into the ligand-mediated synthesis of colloidal $CsPbBr_3$ perovskite nanocrystals: the role of organic acid, base, and cesium precursors. *ACS nano* **2016,** *10* (8), 7943-7954.

41. Ahn N., Son D. Y., Jang I. H., Kang S. M., Choi M., Park N. G., Highly reproducible perovskite solar cells with average efficiency of 18.3% and best efficiency of 19.7% fabricated via Lewis base adduct of lead (II) iodide. *J. Am. Chem. Soc.* **2015,** *137* (27), 8696-8699.

42. Aharon S., Wierzbowska M., Etgar L., The Effect of the Alkylammonium Ligand's Length on Organic–Inorganic Perovskite Nanoparticles. *ACS Energy Lett.* **2018,** *3* (6), 1387-1393.

43. Yassitepe E., Yang Z., Voznyy O., Kim Y., Walters G., Castañeda J. A., Kanjanaboos P., Yuan M., Gong X., Fan F., Osman M. B., Amine‐free synthesis of cesium lead halide perovskite quantum dots for efficient light‐emitting diodes. *Adv. Funct. Mater.* **2016,** *26* (47), 8757-8763.

44. Bansal P., Kar P., Succinic acid-assisted stability enhancement of a colloidal organometal halide perovskite and its application as a fluorescent keypad lock. *New J. chem.* **2019,** *43* (11), 4599-4604.

45. Palazon F., Almeida G., Akkerman Q. A., De Trizio L., Dang Z., Prato M., Manna L., Changing the dimensionality of cesium lead bromide nanocrystals by reversible postsynthesis transformations with amines. *Chem. Mater.* **2017,** *29* (10), 4167-4171.

46. Krieg F., Ochsenbein S. T., Yakunin S., Ten Brinck S., Aellen P., Süess A., Clerc B., Guggisberg D., Nazarenko O., Shynkarenko Y., Maksym V. K., Colloidal $CsPbX_3$ (X= Cl, Br, I) nanocrystals 2.0: Zwitterionic capping ligands for improved durability and stability. *ACS energy lett.* **2018,** *3* (3), 641-646.

47. Wheeler L. M., Sanehira E. M., Marshall A. R., Schulz P., Suri M., Anderson N. C., Christians J. A., Nordlund D., Sokaras D., Kroll T., Targeted Ligand-Exchange

Chemistry on Cesium Lead Halide Perovskite Quantum Dots for High-Efficiency Photovoltaics. *J. Am. Chem. Soc.* **2018,** *140* (33), 10504-10513.

48. Chen F., Wang Y. M., Guo W., Yin X. B., Color-tunable lanthanide metal–organic framework gels. *Chem. sci.* **2019,** *10* (6), 1644-1650.